Hemoglobin-based oxygen carriers camouflaged with membranes extracted from red blood cells: Optimization and assessment of functionality

Jansman, Michelle Maria Theresia; Coll-Satue, Clara; Liu, Xiaoli; Kempen, Paul Joseph; Andresen, Thomas Lars; Thulstrup, Peter Waaben; Hosta-Rigau, Leticia

Published in:
Materials Science and Engineering C

Link to article, DOI:
10.1016/j.msec.2022.112691

Publication date:
2022

Document Version
Publisher's PDF, also known as Version of record

Biomaterials Advances 134 (2022) 112691

Contents lists available at ScienceDirect

Biomaterials Advances

journal homepage: www.elsevier.com/locate/bioadv

Hemoglobin-based oxygen carriers camouflaged with membranes extracted from red blood cells: Optimization and assessment of functionality

Michelle Maria Theresia Jansman [a], Clara Coll-Satue [a], Xiaoli Liu [a], Paul Joseph Kempen [a,b], Thomas Lars Andresen [a], Peter Waaben Thulstrup [c], Leticia Hosta-Rigau [a,*]

[a] Department of Health Technology, Center for Nanomedicine and Theranostics, Technical University of Denmark, Nils Koppels Allé, Building 423, 2800 Kgs. Lyngby, Denmark
[b] DTU Nanolab, National Center for Nano Fabrication and Characterization, Technical University of Denmark, Ørsteds Plads, Building 347, 2800 Kgs. Lyngby, Denmark
[c] Department of Chemistry, University of Copenhagen, Universitetsparken 5, 2100 Copenhagen, Denmark

ARTICLE INFO

Keywords:
Blood substitutes
Hemoglobin-based oxygen carriers
Cerium oxide nanoparticles
Nanozymes
Red blood cell membrane
Reactive oxygen species
Stealth coatings

ABSTRACT

Despite being an indispensable clinical procedure, the transfusion of donor blood has important limitations including a short shelf-life, limited availability and specific storage requirements. Therefore, a lot of effort has been devoted to developing hemoglobin (Hb)-based oxygen carriers (HBOCs) that are able to replace or complement standard blood transfusions, especially in extreme life-threatening situations. Herein, we employed a Hb-loaded poly(lactide-*co*-glycolide) core which was subsequently coated with nanozymes to protect the encapsulated Hb from oxidation by reactive oxygen species. To render HBOCs with long circulation in the vasculature, which is a crucial requirement to achieve the high oxygen demands of our organism, the carrier was coated with a red blood cell-derived membrane. Three coating methods were explored and evaluated by their ability to repel the deposition of proteins and minimize their uptake by an endothelial cell line. Preservation of the oxygen carrying capacity of the membrane-coated carrier was demonstrated by an oxygen-binding and releasing assay and, the functionality resulting from the entrapped nanozymes, was shown by means of superoxide radical anion and hydrogen peroxide depletion assays. All in all, we have demonstrated the potential of the membrane-coated nanocarriers as novel oxygen carrying systems with both antioxidant and stealth properties.

1. Introduction

In order to carry out the basic metabolic activity needed for survival, our body needs a constant supply of oxygen. Blood, which is a complex liquid containing millions of chemicals and cells, is responsible for this task. Specifically, ~98% of oxygen is carried by the red blood cells (RBCs), while the remaining 2% is dissolved in the plasma. Thus, blood loss occurring during e.g., injury and surgery or blood diseases such as hemophilia, ischemia and anemia can have detrimental consequences. In this context, the transfusion of whole blood or, most often, packed RBCs can significantly improve survival.

While blood transfusions are regarded as a safe and well-established procedure, the use of donor blood still presents important limitations [1]. RBCs have a short storage life-time of 42 days at 4 °C and only one day at ambient conditions. RBCs undergo storage lesion over time, which results in morphological changes and hemolysis. The refrigerated storage requirements can become problematic when blood is needed in remote locations. The short life-time furthermore makes the availability of donor blood limited, especially when large amounts are needed at once (e.g., during natural or human-instigated disasters). Thus, with the aim of circumventing the aforementioned limitations of donor blood, a lot of research has been devoted towards creating surrogates of RBCs.

Despite hemoglobin (Hb)'s excellent oxygen carrying and delivering properties, free Hb cannot be directly administered into our body since, once in the bloodstream, it rapidly dissociates into its dimer- and heme-products. Additionally, when excess levels of cell-free Hb are present, the mechanisms to remove Hb's dissociation products (i.e., haptoglobin and hemopexin for dimer- and heme-products, respectively) get saturated [2]. This results in the extravasation of both excess Hb and its dissociation products into the underlying smooth muscle tissue where they scavenge nitric oxide (NO). Since NO is an important vasodilator, NO removal results in vasoconstriction, inflammation and coagulation [2,3]. Thus, strategies to eliminate Hb's toxicity while preserving its oxygen carrying ability are being developed giving rise to the so-called Hb-based oxygen carriers (HBOCs). Specifically, HBOCs are being fabricated by chemically modifying Hb to form complexes or by entrapping Hb within an encapsulation platform [4]. For both strategies, the aim is to increase the molecular dimensions of Hb and to shield it from extravasation in between the cells lining of the blood vessels into the smooth muscle tissue.

Another important challenge to address when developing HBOCs, is the oxidation of Hb into non-functional methemoglobin (metHb), a process that gets exacerbated in the presence of reactive oxygen species (ROS) such as superoxide radical anion ($O_2^{\bullet -}$) and hydrogen peroxide (H_2O_2) [5]. Within

* Corresponding author.
E-mail address: leri@dtu.dk (L. Hosta-Rigau).

http://dx.doi.org/10.1016/j.msec.2022.112691
Received 1 September 2021; Received in revised form 13 January 2022; Accepted 28 January 2022
Available online 3 February 2022

RBCs, Hb oxidation is prevented and/or reversed by an intricate antioxidant system. Two prominent components of this system are the enzymes superoxide dismutase (SOD) and catalase (CAT). While SOD catalyzes the reduction of $O_2^{\bullet -}$ into H_2O_2, CAT has the ability to disproportionate H_2O_2 into oxygen and water. Even though this enzymatic system inspired multiple research groups to incorporate SOD and CAT within their HBOCs, employing natural enzymes comes with important limitations [6–8]. These include high production costs, limited catalytic active sites and half-lives, as well as batch-to-batch variation. Furthermore, modification of the enzymes structure (e.g., following chemical modification or encapsulation with HBOCs) results in alteration of their functionality [9]. Thus, to create HBOCs with antioxidant properties, the incorporation of nanozymes (NZs), which are nanoparticles (NPs) displaying catalytic properties, has emerged as an interesting alternative. When compared to native enzymes, NZs have higher stability and opportunity for modification without compromising their function [10]. Additionally, NZs experience better recyclability over their natural counterparts, which is a critical aspect if they are expected to perform for an extended period of time. However, while NZs have been widely explored in the context of drug delivery or tissue engineering, their use in the field of blood substitutes has been rather limited [11,12]. Specifically, Hosaka et al. made use of platinum NPs (Pt-NPs) as antioxidant NZs and incorporated them within a novel HBOC consisting of a protein cluster composed of Hb and human serum albumin [13]. As a result of the high catalytic activity of the Pt-NPs (i.e., the NZs) the autoxidation of Hb into metHb was minimized, even in the presence of ROS. We have also reported the fabrication of HBOCs containing NZs. In particular, we employed cerium oxide NPs (CeO_2-NPs) to decorate a HBOC consisting of a Hb-containing poly(lactide-*co*-glycolide) (PLGA) core which was subsequently decorated with polyethylene glycol (PEG) [14,15]. While, by means of the NZs, the resulting HBOC had the ability to deplete both $O_2^{\bullet -}$ and H_2O_2 in a sustained manner; as a result of the PEG coating, decreased cell uptake by endothelial cells and macrophages was achieved. This is an important aspect, since an ever-present concern when developing HBOCs is to achieve long circulation in the bloodstream, which is essential to attain the high oxygen demands of our body. While the golden standard to render intravenously administered carriers with stealth properties is the functionalization with PEG, the production of anti-PEG antibodies is an increasingly recognized issue [16]. The creation of PEG antibodies results in the recognition and subsequent elimination of PEGylated drugs or NPs by the mononuclear phagocyte system (MPS) in the liver and spleen. To circumvent this drawback, alternatives to PEGylation are highly sought after [17,18]. A promising approach is the coating with membranes extracted from biological RBCs. RBCs are nature's long circulating carriers, since by a combination of a surface makeup involving proteins and glycans together with their size, shape and elasticity, RBCs can stay in circulation for up to 120 days. Specifically, the glycoprotein CD47 and sialyl residues located in the outer part of the RBCs membrane play a major role in this context. While CD47 inhibits the uptake by the MPS by transducing an inhibitory signal to phagocytes, sialic acid is also a determinant for the RBCs' life span since desialylated RBCs are rapidly sequestered in the liver and spleen [19–21].

Thus, the objective of this work is to further improve the stealth properties of our previously developed HBOC by replacing the PEG coating by a RBC membrane (RBC-M) coating. In order to achieve this goal, we make use of HBOCs consisting of Hb-loaded PLGA-NPs decorated with NZs and explore three different methods to coat them with membranes extracted from RBCs (Scheme 1A). The resulting coatings are evaluated by their ability to minimize protein adsorption (i.e., opsonization) and to diminish their uptake by an endothelial cell line. The functionality of the membrane-coated carrier is next assessed by its ability to bind and release oxygen and to scavenge two harmful ROS as a result of the embedded NZs (Scheme 1B). Lastly, the bio- and hemocompatibility of the nanocarriers is also evaluated.

2. Materials and methods

2.1. Materials

Phosphate buffer saline (PBS), tris(hydroxymethyl) aminomethane (TRIS), sodium chloride (NaCl), ammonia (25% solution), hydrochloric

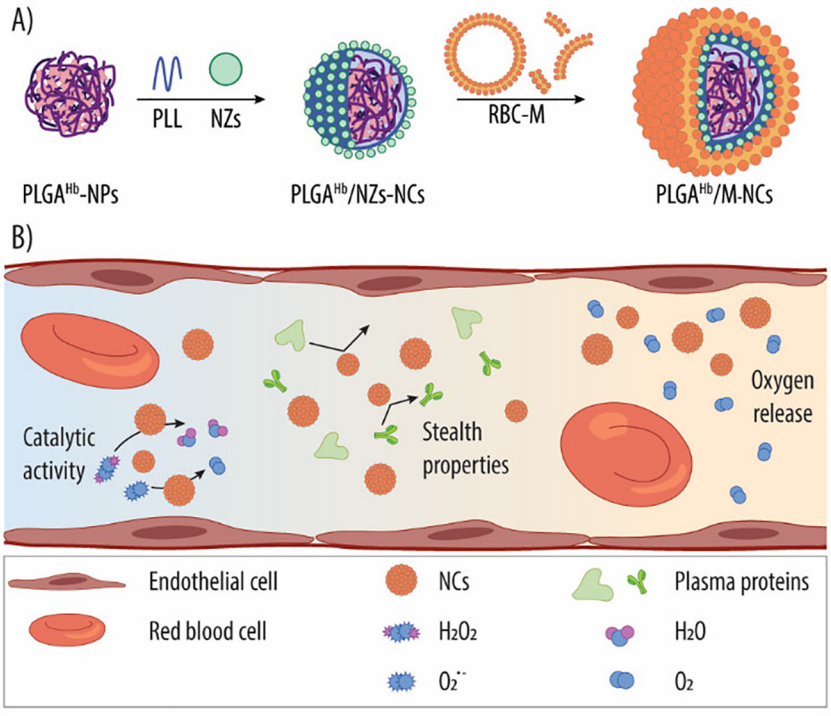

Scheme 1. Illustration of the NCs' fabrication and functionality. A) $PLGA^{Hb}$-NPs were coated with poly(L-lysine) (PLL), nanozymes (NZs) and red blood cell membrane (RBC-M) to obtain multifaceted NCs. B) The encapsulation of NZs provides catalytic activity towards reactive oxygen species (i.e., hydrogen peroxide (H_2O_2) and superoxide radical anion ($O_2^{\bullet -}$)) to protect Hb's functionality to delivery oxygen, while the RBC-M coating provides stealth properties against protein adsorption.

acid (HCl), nitric acid (HNO_3), ethylenediaminetetraacetic acid (EDTA) solution, H_2O_2, citric acid, PLGA (50:50, M_W 30–60 kDa), poly(vinyl alcohol) (PVA, M_W 13–23 kDa), poly(L-lysine) (PLL, M_W 30–70 kDa), cerium(III) nitrate hexahydrate ($Ce(NO_3)_3{\cdot}6H_2O$), iridium and cerium standards for ICP-MS, fluorescein isothiocyanate (FITC)-labeled immunoglobulin G (IgG) (IgG^F) from human serum, xanthine, xanthine oxidase (XO) from bovine milk, horseradish peroxidase (HRP), CAT from bovine liver, SOD from bovine erythrocytes, cell proliferation reagent WST-1, dimethyl sulfoxide (DMSO), sodium dithionite (SDT), human umbilical vein endothelial cell line (HUVEC) and trypsin were purchased from Merck Life Science A/S (Søborg, DK). Bovine blood with citrate was purchased from SSI Diagnostica A/S (Hillerød, DK). Organic solvents were purchased from VWR International A/S (Søborg, DK). 1,1′-Dioctadecyl-3,3,3′,3′-tetramethylindodicarbocyanine perchlorate (DiD), 1,1′-dioctadecyl-3,3,3′,3′-tetramethylindocarbocyanine perchlorate (DiI), Pierce™ bicinchoninic acid (BCA) protein assay kit, Whatman™ Nuclepore™ 1 μm polycarbonate membranes, Amplex™ Red reagent and PrestoBlue were purchased from ThermoFisher Scientific (Waltham, MA, USA). Amicon centrifugal filter units (100 kD MWCO) were purchased from Th. Geyer Skandinavien ApS (Roskilde, DK). Endothelial cell medium (ECM) kit including fetal bovine serum (FBS), penicillin/streptomycin solution and endothelial cell growth supplement was purchased from Innoprot (Derio-Biskaia, ES).

TRIS 1 buffer contains 10 mM TRIS (pH 8.5). TRIS 2 buffer contains 10 mM TRIS and 150 mM NaCl (pH 7.4). The buffers were prepared using ultrapure water (Milli-Q (MQ), EMD Millipore, USA).

Bare PLGA-NPs and FITC-labeled bovine serum albumin (BSA^F) were prepared according to previous reported protocols [14,22].

2.1.1. Hb extraction from bovine blood

Hb was extracted from bovine RBCs following a reported protocol [23]. In short, whole bovine blood was washed in a 0.9% NaCl solution (3×, 2000*g*, 20 min, 4 °C, 1:1 v/v ratio) using a high-speed centrifuge (SL16R centrifuge, ThermoScientific). The resulting pellet containing the RBCs was thoroughly mixed with MQ and toluene (1:1:0.4 volume ratio) to lyse the cells. The overnight storage (4 °C) allowed for the separation of the stroma-free Hb phase. The Hb phase was collected, spun down (8000*g*, 20 min) and filtered through ash-free paper before storage at −80 °C. A BCA protein assay kit was used to determine the Hb concentration of the obtained solution.

2.1.2. Extraction of RBC-Ms from human blood

Human blood was withdrawn from healthy donors in the Department of Health Technology at Technical University of Denmark (Kongens Lyngby, DK) according to the rules of the Danish National Committee for Ethics in Science. The donors provided their informed consent to participate and all the operators received appropriate training to handle the biological materials used in this study.

The RBC-Ms were isolated from human blood according to Liu et al. [24] Specifically, whole blood from healthy donors was collected in heparin-coated tubes and washed in PBS (3×, 1500*g*, 15 min, 4 °C) to remove the blood serum and buffy coat. The resulting blood cells were subsequently washed in a hypotonic medium (PBS:MQ 1:4 volume ratio) to remove the intracellular contents (5×, 15,000*g*, 20 min, 4 °C). The obtained light pink pellet containing the RBC-Ms was resuspended in hypotonic medium until reaching the same volume of the extracted donor blood. The RBC-Ms were aliquoted and stored at −20 °C.

To obtain fluorescently labeled RBC-Ms ($RBC\text{-}M^F$s), 10 μL DiD (1 mg mL^{-1} in DMSO, $\lambda_{ex}/\lambda_{em}$ = 644/665 nm) was added to a suspension of RBC-Ms (1 mL, extracted from 1 mL donor blood) and incubated for 30 min in a tube rotator. The $RBC\text{-}M^F$s were washed in TRIS 1 (2×, 6500*g*, 10 min) using Amicon centrifugal filters to remove excess DiD and re-suspended in TRIS 1.

2.1.3. Cell culture

HUVEC cells were cultured in ECM supplemented with FBS (5% v/v), penicillin/streptomycin (1% v/v, 10,000 U mL^{-1} and 0.01 mg mL^{-1}, respectively) and endothelial cell growth supplement (1% v/v). The cells were cultured at 37 °C in a humidified incubator with 5% CO_2.

2.2. Fabrication and characterization of the different components of the nanocarriers (NCs)

2.2.1. Hb-loaded PLGA-NPs ($PLGA^{Hb}$-NPs)

$PLGA^{Hb}$-NPs were prepared using a double emulsion solvent evaporation method. Briefly, 250 μL Hb (75 mg mL^{-1} in PBS) was added to 2 mL PLGA (5 mg mL^{-1} in DCM) followed by sonication (70% amplitude, 40 s, 1 s/1 s) (Q700 sonicator with microprobe, Qsonica) on ice. The obtained emulsion was added to 10 mL PVA (10 mg mL^{-1} in MQ) followed by sonication to yield a double emulsion, which was stirred for 30 min followed by rotary evaporation to remove the DCM. The resulting $PLGA^{Hb}$-NPs were washed in TRIS 1 (2×, 6500*g*, 10 min, 4 °C). The concentration of $PLGA^{Hb}$-NPs was determined by lyophilizing an aliquot of sample.

To obtain fluorescently labeled $PLGA^{Hb}$-NPs ($PLGA^{F/Hb}$-NPs), 3 μL DiI (2 mg mL^{-1} in *tert*-butanol:MQ 9:1 volume ratio, $\lambda_{ex}/\lambda_{em}$ = 549/565 nm) was added to the DCM phase. $PLGA^{F/Hb}$-NPs were used in experiments where quantification of the NCs was required. The concentration of $PLGA^{F/Hb}$-NPs was determined by lyophilizing an aliquot of the sample. The fluorescence intensity (FI) of the sample was measured using a plate reader (Tecan Spark, Tecan Group Ltd., Männedorf, CH) and correlated to the concentration of $PLGA^{F/Hb}$-NPs.

The hydrodynamic size and polydispersity index (PDI) of the $PLGA^{Hb}$-NPs were evaluated by dynamic light scattering (DLS) (Zetasizer Nanoseries nano-ZS, Malvern Panalytical Ltd., Malvern, UK). The Zetasizer was furthermore employed to assess the zeta (ζ)-potential.

The loading capacity of the $PLGA^{Hb}$-NPs was determined as a weight ratio and calculated as:

$$\text{LC}\ (\%) = \left(\text{amount of entrapped Hb/final amount of } PLGA^{Hb}\text{−NPs}\right) \times 100. \quad (1)$$

The amount of encapsulated Hb (mg) was evaluated by absorbance (Abs) measurements of the Soret peak (~414 nm) using UV–Vis spectroscopy (NanoDrop 2000c, ThermoFisher Scientific, Waltham, USA). The background slope (due to bare PLGA-NPs) was removed and the Abs value was correlated to a Hb standard curve. The total amount of $PLGA^{Hb}$-NPs (mg) was determined by lyophilizing an aliquot of the $PLGA^{Hb}$-NPs sample.

2.2.2. CeO_2-NPs, NZs

Citrate-capped CeO_2-NPs were prepared according to a previous reported protocol [14,25]. In short, 12.5 mL of a $Ce(NO_3)_3{\cdot}6\ H_2O$ solution (21.71 mg mL^{-1} in MQ) was mixed with citric acid (120 mg) and subsequently poured into 50 mL of an ammonia solution (3 M). The resulting mixture was allowed to react for 2 h and the obtained CeO_2-NPs were precipitated using ~25 mL HCl (5 M). The CeO_2-NPs were then left to sediment and washed in 40 mL MQ (3×) and re-suspended in increasing amounts of an ammonia solution (1 M) until reaching neutral pH. All glassware was cleaned with Aqua Regia (HNO_3:HCl, 1:3 M ratio) prior to use.

Inductively coupled plasma mass spectrometry (ICP-MS) (iCAPQ, ThermoFisher Scientific, Waltham, USA) was employed to assess the cerium content of the NZs suspensions. For faster quantification, the concentrations obtained by ICP-MS were correlated to the Abs readings of the NZs at 350 nm by the NanoDrop [14].

2.3. NCs fabrication and characterization

2.3.1. NCs assembly

The LbL technique was used to adsorb the NZs onto the $PLGA^{Hb}$-NPs. First, 150 μL of PLL (1 mg mL^{-1}) was added to a suspension of $PLGA^{Hb}$-NPs (1000 μg in 150 μL TRIS 1) and incubated for 10 min. The resulting NCs ($PLGA^{Hb}$/PLL-NCs) were washed in TRIS 1 (2×, 4847*g*, 4 min) using a bench-top centrifuge (MiniSpin, Eppendorf AG, Hamburg, DE) and

resuspended in 150 μL TRIS 1. Next, 150 μL of NZs (25 mM) was added to the PLGA^{Hb}/PLL-NPs followed by 10 min incubation and subsequent washing in TRIS 1 (2×, 4847*g*, 4 min). The resulting PLGA^{Hb}/NZs-NCs were resuspended in 150 μL TRIS 1.

The ζ-potentials of the resulting NCs were evaluated using the Zetasizer. The hydrodynamic size of the uncoated PLGA^{Hb}-NPs and after the deposition of PLL and NZs (PLGA^{Hb}/NZs-NCs) was assessed using nanoparticle tracking analysis using a ZetaView PMX120 instrument (Particle Metrix GmbH, DE). Measurements were performed at 11 different positions with a sensitivity of 60, a shutter value of 100 and a frame rate of 7.5. The obtained histograms were smoothened using adjacent-averaging with a 7-point window (OriginPro 2019 software).

2.3.2. Cryogenic transmission electron microscopy (cryoTEM)

CryoTEM images of the PLGA^{Hb}-NPs and PLGA^{Hb}/NZs-NCs were obtained using a Tecnai T20 G2 (Thermo Fisher Scientific, Waltham, USA) operating at 200 kV and located at the Center for Integrated Microscopy at the University of Copenhagen. Images were acquired in low dose mode using a FEI High Sensitive 4 k × 4 k Eagle camera. 3 μL of solution was drop cast onto a freshly glow discharged lacy carbon 300 mesh copper TEM grid (Ted Pella Inc., Redding, CA, USA) and plunge frozen in liquid ethane using a FEI Vitrobot Mark IV (Thermo Fisher Scientific, Waltham, USA).

2.4. NCs coating with RBC-Ms

Three different methods based on extrusion, sonication, or their combination were investigated to coat the PLGA^{Hb}/NZs-NCs with RBC-Ms, thus rendering PLGA^{Hb}/M-NCs.

2.4.1. Extrusion method

The NCs coated by this method (PLGA^{Hb}/M^{Extr}-NCs) were prepared following reported protocols with minor modifications [26,27]. RBC-M-vesicles (RBC-MVs) were first prepared by sonicating the RBC-Ms (1 mL, extracted from 1 mL donor blood) on ice (70% amplitude, 10 s, 1 s/1 s) followed by extrusion through 1 μm polycarbonate membrane using a Mini-Extruder set (Avanti Polar Lipids, Inc., AL, USA). Next, 150 μL of a suspension of PLGA^{Hb}/NZs-NCs (prepared from 1000 μg PLGA^{Hb}-NPs as starting material) was added to increasing amounts of RBC-MVs (0–800 μL RBC-MVs, extracted from 0 to 800 μL donor blood) and TRIS 1 was added to the mixture to a final volume of 1 mL. The resulting suspension was vortexed and extruded through a 1 μm polycarbonate membrane to obtain PLGA^{Hb}/M^{Extr}-NCs which were subsequently washed in TRIS 1 (2×, 5433*g*, 4 min) using the bench-top centrifuge to eliminate the unbound RBC-MVs.

2.4.2. Sonication method

The NCs coated by this method (PLGA^{Hb}/M^{Sonic}-NCs) were fabricated as described by Ben-Akiva et al. with some minor adjustments [28]. Prior to coating the NCs, the RBC-Ms were sonicated on ice (50%, 2 min, 1 s/1 s) to create RBC-M fragments. Next, 150 μL PLGA^{Hb}/NZs-NCs (fabricated from 1000 μg PLGA^{Hb}-NPs as starting material) was added to 0–800 μL of fragmented RBC-Ms (extracted from 0 to 800 μL of donor blood) and TRIS 1 was added to the mixture to a final volume of 1 mL. The resulting suspension was vortexed and sonicated on ice (50%, 2 min, 1 s/1 s) to obtain PLGA^{Hb}/M^{Sonic}-NCs. The NCs were washed in TRIS 1 (2×, 5433*g*, 4 min) to eliminate unbound RBC-Ms.

2.4.3. Combination method

The NCs coated by the combination method (PLGA^{Hb}/M^{Comb}-NCs) were assembled with minor modifications of our protocol [24]. 150 μL PLGA^{Hb}/NZs-NCs (fabricated from 1000 μg PLGA^{Hb}-NPs as starting material) was added to 0–800 μL of RBC-Ms (extracted from 0 to 800 μL of donor blood) followed by the addition of TRIS 1 to a final volume of 1 mL. The mixture was vortexed and sonicated on ice (70%, 10 s, 1 s/1 s), followed by extrusion using a 1 μm polycarbonate membrane and the mini-extruder set. The coated PLGA^{Hb}/M^{Comb}-NCs were washed in TRIS 1 (2×, 5433*g*, 4 min).

2.4.4. Characterization of RBC-M coating

The three different PLGA^{Hb}/M-NCs assembled with increasing amounts of RBC-Ms (0–400 μL, extracted from 0 to 400 μL donor blood) were first evaluated using the fluorescently labeled RBC-M^{F}s. After fabrication, the FI of the NCs was analyzed using a BD Accuri C6 flow cytometer (BD Biosciences, Sparks, MD, USA). As controls, physical mixtures of PLGA^{Hb}/NZs-NCs and RBC-M^{F} (0–400 μL, extracted from 0 to 400 μL of donor blood) were prepared and analyzed. Two independent experiments were carried out.

The PLGA^{Hb}/NZs-NCs and PLGA^{Hb}/M-NCs suspensions prepared with the three different coating methods and using 800 μL of RBC-Ms were visualized by differential interference contrast (DIC) microscopy (Olympus Inverted IX83, 60× oil objective).

TEM imaging was performed to examine the structure of the PLGA^{Hb}/NZs-NCs and the PLGA^{Hb}/M-NCs (assembled using 800 μL of RBC-Ms) by the three different methods. For that, 3 μL of solution was drop cast onto a freshly glow discharged TEM grid and allowed to adsorb for 5 min before removing the excess solution. The grid was then rinsed with distilled water 3 times and placed on a drop of 2% uranyl acetate stain for 30 s before the excess was wicked away with filter paper to negatively stain the sample. The grid was dried and imaged using a Tecnai T20 G2 located at the National Centre for Fabrication and Characterization at Technical University of Denmark. Images were acquired using a TVIPS-XF416 CMOS camera (TVIPS GmbH, Gauting, DE).

2.5. Evaluation of the stealth properties

The stealth properties of the three different PLGA^{Hb}/M-NCs as a result of the coating by the RBC-Ms were assessed by a protein binding assay. Fluorescently labeled PLGA$^{F/Hb}$-NPs were used to quantify the amount of NCs needed for the assay. PLGA$^{F/Hb}$/M-NCs were prepared using increasing amounts of RBC-Ms (0–800 μL of RBC-Ms) and the three different coating methods (i.e., extrusion: PLGA^{Hb}/M^{Extr}-NCs; sonication: PLGA^{Hb}/M^{Sonic}-NCs; and combination: PLGA^{Hb}/M^{Comb}-NCs). Equal amounts of the NCs (200 μg dispersed in 150 μL TRIS 2) were incubated with an IgG^{F} or BSA^{F} solution (50 μL, 2.0 mg mL^{-1} in TRIS 2) for 4 h using a thermoshaker (PHMT Thermoshaker, Grant-bio, UK) at 37 °C and a shaking speed of 1200 rpm. The samples were then washed in TRIS 2 (2×, 5433*g*, 4 min) and the FI of the adsorbed fluorescently labeled proteins was evaluated using the flow cytometer ($\lambda_{ex}/\lambda_{em}$ = 488/533 nm). The FI was normalized (nFI) to the uncoated PLGA$^{F/Hb}$/NZs-NCs.

2.6. Evaluation of the oxygen-binding and releasing properties

2.6.1. Circular dichroism (CD)

The CD spectra were obtained using a Jasco J-815 spectropolarimeter (JASCO, Essex, UK). PLGA^{Hb}-NPs, PLGA^{Hb}/PLL-NCs, PLGA^{Hb}/NZs-NCs and the PLGA^{Hb}/M-NCs assembled by the three different methods (i.e., PLGA^{Hb}/M^{Extr}-NCs, PLGA^{Hb}/M^{Sonic}-NCs and PLGA^{Hb}/M^{Comb}-NCs) all at a concentration of ~0.04 mg mL^{-1} protein content in TRIS 1, were evaluated using a 0.5 mm quartz cuvette. Free Hb, RBC-Ms (both at 0.04 mg mL^{-1}) and TRIS 1 were used as controls. Each spectrum was collected as an average of ten scans and the spectrum of the control sample was subtracted (i.e., TRIS 1). The spectra were smoothed using the Jasco software and normalized to the lowest band of the Hb spectrum.

2.6.2. Oxygen-binding and releasing study

To assess the functionality of the NCs, an oxygen-binding and release study was conducted using an UV–Vis spectrophotometer (UV-2600, Shimadzu Corp., Kyoto, JP). As a first step, the UV–Vis spectrum of the PLGA^{Hb}-NPs (2.5 mL, 0.5 mg mL^{-1}) was evaluated using PLGA-NPs (2.5 mL, 0.2 mg mL^{-1}) as a reference. Next, the PLGA^{Hb}-NPs were exposed to nitrogen gas (N_2) for 10 min, followed by adding a pinch of SDT to remove any residual oxygen prior to recording the spectrum of the resulting deoxygenated Hb (deoxy-Hb). Subsequently, the PLGA^{Hb}-NPs were exposed to a flow of air for 10 min and the spectrum resulting from the oxygenated Hb

(oxy-Hb) was recorded. Lastly, one additional round of N_2 purging and recording was conducted.

The oxygen-releasing properties of the coated PLGA^{Hb}/M-NCs assembled by the three different methods (i.e., extrusion: PLGA^{Hb}/M^{Extr}-NCs; sonication: PLGA^{Hb}/M^{Sonic}-NCs; and combination: PLGA^{Hb}/M^{Comb}-NCs) were also assessed but using TRIS 1 as a reference. For that, the NCs were evaluated in their oxy-Hb and deoxy-Hb state using N_2 purging for 10 min and adding a pinch of SDT.

2.7. ROS scavenging properties

2.7.1. Scavenging properties of the CeO_2-NPs

2.7.1.1. Scavenging of $O_2^{\bullet -}$. The WST-1 assay was employed to evaluate the depletion of $O_2^{\bullet -}$ by the NZs and the corresponding native enzyme (i.e., SOD). Specifically, 200 μL of a reagent mixture containing WST-1 (2.5% v/v), EDTA (0.1 mM) and xanthine (0.1 mM) was added to 100 μL NZs (0–4 mM) or SOD (0–500 U mL^{-1}), all in TRIS 1. To start the reaction, 10 μL XO (0.05 U mL^{-1}) was added to the suspension followed by 30 min incubation in the thermoshaker. Next, 180 μL was transferred to a 96-well plate and the Abs was measured at 438 nm using the plate reader. TRIS 1 (100 μL) mixed with reagent mixture (200 μL) with and without the addition of XO were used as positive and negative controls, respectively. The normalized Abs (nAbs) was calculated as:

$$\text{nAbs}(\%) = (\text{experimental value} - \text{negative control}) \div (\text{positive control} - \text{negative control}) \times 100. \quad (2)$$

2.7.1.2. Scavenging of H_2O_2. The Amplex Red assay was employed to evaluate the depletion of H_2O_2 by the NZs and the corresponding native enzyme (i.e., CAT). For this, 10 μL H_2O_2 (0.09 mM) was added to 100 μL of NZs (0–4 mM) or CAT (0–15 U mL^{-1}), all in TRIS 1. The mixture was incubated for 15 min in the thermoshaker. Next, 100 μL HRP (2 U mL^{-1}) and 10 μL Amplex Red (0.1 mM) were added and the suspensions were incubated for 5 additional min in the thermoshaker. Next, 180 μL was transferred to a black 96-well plate to measure the FI (resorufin product: $\lambda_{ex}/\lambda_{em}$ = 530/586 nm) using the plate reader. 100 μL TRIS 1, with and without 10 μL H_2O_2 (0.09 mM), were used as positive and negative controls, respectively. The nFI was calculated as:

$$\text{nFI}(\%) = (\text{experimental value} - \text{negative control}) \div (\text{positive control} - \text{negative control}) \times 100. \quad (3)$$

2.7.1.3. Stability over time. Stock suspensions of NZs (20 mM), SOD (2000 U mL^{-1}) and CAT (200 U mL^{-1}) were stored at 4 °C, at room temperature (RT) and 37 °C. On predetermined days, 5 μL aliquots of the solutions were taken and the ability of the NZs and the enzymes to deplete $O_2^{\bullet -}$ or H_2O_2 was evaluated using the WST-1 and Amplex Red assays. For the WST-1 assay the aliquots of NZs or SOD were added to 95 μL TRIS 1 to obtain 100 μL of 1 mM NZs or 100 U mL^{-1} SOD, respectively. The WST-1 assay was then performed as described above (Section 2.7.1.1). For the Amplex Red assay the aliquots of NZs or CAT were diluted in TRIS 1 to obtain 100 μL of 1 mM NZs or 10 U mL^{-1} CAT, respectively and the assay was performed as described above (Section 2.7.1.2).

2.7.2. Scavenging properties of the NCs

2.7.2.1. Scavenging of $O_2^{\bullet -}$. The WST-1 assay was also used to evaluate the catalytic activity of the NCs at different stages of the assembly process (i.e., PLGA$^{F/Hb}$-NPs, PLGA$^{F/Hb}$/NZs-NCs, PLGA$^{F/Hb}$/M^{Extr}-NCs, PLGA$^{F/Hb}$/M^{Sonic}-NCs and PLGA$^{F/Hb}$/M^{Comb}-NCs). For that, 100 μL of a NCs suspension (0–200 μg) was mixed with 100 μL of a reagent mixture containing WST-1 (2.5% v/v), EDTA (0.1 mM) and xanthine (0.1 mM), all in TRIS 1. To start the reaction, 10 μL XO (0.025 U mL^{-1}) was added to the mixture, followed by 30 min incubation in the thermoshaker. Then, the NCs were spun down (5433*g*, 4 min) and 180 μL supernatant of each sample was transferred to a 96-well plate and measured in the plate reader. The Abs was measured at 438 nm. TRIS 1 (100 μL) mixed with reagent mixture (100 μL) with and without the addition of XO were used as positive and negative controls, respectively. The nAbs was calculated according to Eq. (2).

To conduct multiple cycles of $O_2^{\bullet -}$ scavenging, the reaction was performed using Amicon centrifugal filter units [29]. The filters act as reaction containers that make it possible to remove the xanthine, EDTA and WST-1 reagents as filtrates by centrifugation while simultaneously minimizing NCs loss during the washing steps. Removal of xanthine and WST-1 is necessary to avoid interference during the subsequent cycles. After the 30 min incubation in the thermoshaker, the suspensions were spun down (15,000*g*, 3 min) and 150 μL of filtrate was used to measure the Abs at 438 nm. The NCs collected in the filter were washed with TRIS 1 (2×, 15,000*g*, 3 min) and incubated again with fresh TRIS 1, XO and reagent mixture to initiate the next cycle of $O_2^{\bullet -}$ scavenging. The NCs activity was assessed for four subsequent cycles.

2.7.2.2. Scavenging of H_2O_2. The Amplex Red assay was also used to evaluate the activity of the NCs at different stages of the assembly process (i.e., PLGA$^{F/Hb}$-NPs, PLGA$^{F/Hb}$/NZs-NCs, PLGA$^{F/Hb}$/M^{Extr}-NCs, PLGA$^{F/Hb}$/M^{Sonic}-NCs and PLGA$^{F/Hb}$/M^{Comb}-NCs). For that, 10 μL H_2O_2 (0.45 mM) was added to 200 μL of a NCs suspension (0–200 μg), all in TRIS 1, followed by a 15 min incubation in the thermoshaker. The NCs were spun down (5433*g*, 4 min) and 180 μL of the supernatant of each sample was transferred to a new tube. To this, 100 μL HRP (2 U mL^{-1}) and 10 μL Amplex Red (0.1 mM), all in TRIS 1, were added followed by 5 min incubation in the thermoshaker. Next, 180 μL was transferred to a black 96-well plate to measure the FI (resorufin product: $\lambda_{ex}/\lambda_{em}$ = 530/586 nm) using the plate reader. 200 μL TRIS 1, with and without 10 μL H_2O_2 (0.45 mM), were used as positive and negative controls, respectively. The nFI was calculated according to Eq. (3).

To conduct additional cycles of H_2O_2 scavenging, the pellets containing the NCs were resuspended in 180 μL of fresh TRIS 1 and 10 μL H_2O_2 (0.45 mM) was added again to initiate the next scavenging cycle. Furthermore, for each new cycle, fresh positive and negative controls were prepared. The NCs activity was assessed for four subsequent cycles.

2.8. Biocompatibility

2.8.1. Hemolysis rate

To assess the hemocompatibility of the NCs (i.e., PLGA$^{F/Hb}$/NZs-NCs, PLGA$^{F/Hb}$/M^{Extr}-NCs, PLGA$^{F/Hb}$/M^{Sonic}-NCs and PLGA$^{F/Hb}$/M^{Comb}-NCs) a hemolysis rate test was performed. Whole blood from healthy donors was collected in heparin-coated collection tubes and washed in PBS (3×, 1000*g*, 15 min, 4 °C) followed by a 50× dilution using PBS. Next, 200 μL of diluted blood was added to a NCs suspension (300 μL, 0–200 μg in PBS) and incubated for 2 h using a thermoshaker (with gentle shaking). After incubation, two centrifugation steps were conducted. The suspension was spun down at 1000*g*, 10 min, 200 μL of supernatant was transferred to a new tube and spun down again at 5433*g*, 4 min. 100 μL of the new supernatant was transferred to a 96-well plate to measure the Abs at 540 nm. The hemolysis rate was calculated using Eq. (2). As positive and negative controls, 200 μL of diluted blood was added to 300 μL of MQ and PBS, respectively.

2.8.2. Cell viability

The biocompatibility of the NCs (PLGA$^{F/Hb}$/NZs-NCs, PLGA$^{F/Hb}$/M^{Extr}-NCs, PLGA$^{F/Hb}$/M^{Sonic}-NCs and PLGA$^{F/Hb}$/M^{Comb}-NCs) was furthermore assessed by a cell viability assay using the HUVEC endothelial cell line. For this, 15,000 cells per well were seeded in a 96-well plate. The cells were allowed to attach for 24 h, followed by washing in PBS (2×, 200 μL) and the addition of various amounts of NCs (200 μL, 0–200 μg in cell

media). After 4 h of incubation, the cells were washed in PBS (3×, 200 μL) and PrestoBlue (100 μL, 10% v/v in cell media) was added. After 1 h incubation, the supernatants were transferred to a 96-well plate to measure the FI of the resazurin product ($\lambda_{ex}/\lambda_{em}$: 535/615 nm). Cells only and cell media were used as positive and negative control, respectively and used to calculate the normalized cell viability (nCV).

2.8.3. Cell association/uptake study

HUVECs were also used to assess the NCs' association/uptake. 15,000 cells per well were seeded in a 96-well plate. The cells were allowed to attach for 24 h, followed by washing in PBS (2×, 200 μL) and the addition of various amounts of NCs (200 μL, 0–200 μg in cell media). After 2 h of incubation, the cells were washed with PBS (3×, 200 μL) and 60 μL trypsin was added to detach the cells. After the cells had detached, 150 μL of FBS-free medium was added to the cells and the cell suspensions were transferred to a round-bottom 96-well plate. The cells were washed in PBS (3×, 300*g*, 5 min) prior to the measuring their FI using the flow cytometer. The cell uptake/association was determined by the cell mean FI (CMFI), which was normalized to the CMFI (nCMFI) of the PLGA$^{F/Hb}$/NZs-NCs at a concentration 1×.

2.9. Statistical analysis

Statistical analysis between different conditions was performed using OriginPro software (OriginLab). A one-way ANOVA with confidence level of 95% ($\alpha = 0.05\%$) using the Dunnett test. $^{*}p \leq 0.05$, $^{**}p \leq 0.01$, $^{***}p \leq 0.001$.

3. Results and discussion

3.1. NCs assembly and characterization

We have previously reported the encapsulation of Hb within a PLGA-NP core to obtain PLGA^{Hb}-NPs, showing that changing the fabricating parameters resulted in the encapsulation of functional Hb with good LC and size distribution of the NPs [15]. On a different study, to protect the Hb against oxidation into the nonfunctional metHb, we investigated the incorporation of CeO_2-NPs as NZs [14]. NZs are a novel class of NP systems that display catalytic activity such as the scavenging of $O_2^{\bullet -}$ and H_2O_2, without having the limitations of native enzymes, which include high production costs, short half-lives, or environmental sensitivity [10]. Furthermore, the NZs can be easily prepared. Thus, herein we prepare PLGA^{Hb}-NPs to subsequently decorate them with NZs. The as-synthetized PLGA^{Hb}-NPs displayed a hydrodynamic size of around 310 nm, a PDI of 0.16 and a ζ-potential of −23 mV. These values are similar to our previously reported PLGA^{Hb}-NPs [15]. The LC, measured as the amount of Hb within the total amount of PLGA^{Hb}-NPs, was calculated to be 22 ± 3%. In order to incorporate the NZs, a positively charged PLL layer was first adsorbed onto the NCs for charge reversal since the NZs have a negative ζ-potential of −26 ± 7 mV (Fig. 1A). While PLL adsorption resulted in PLGA^{Hb}/PLL-NCs with a ζ-potential of 20 ± 1 mV, the deposition of NZs was confirmed by a decrease in ζ-potential to −19 ± 2 mV. The incorporation of PLL and NZs resulted in an average increase of 20 nm in hydrodynamic size (Fig. 1B). The successful incorporation of the NZs to render PLGA^{Hb}/NZs-NCs was furthermore confirmed by cryoTEM imaging (Fig. 1C). Prior incorporation of the NZs, the PLGA^{Hb}-NPs were smooth in appearance. However, as shown by the multiple black dots, the deposition of the NZs was uniform and almost fully covering the NCs.

To meet the high oxygen demands of our body, HBOCs need to display extended circulation times in the vasculature. The most common approach to fabricate long-circulating NPs is to decorate their surface with PEG [30–32]. The so-called PEGylation strategy reduces the adsorption of plasma proteins on the NPs' surface, thereby protecting them from recognition by the MPS [33]. However, the increased exposure to PEG-containing medicines and daily products can result in the production of anti-PEG antibodies which enhance the recognition of the coated NPs by the MPS, thus

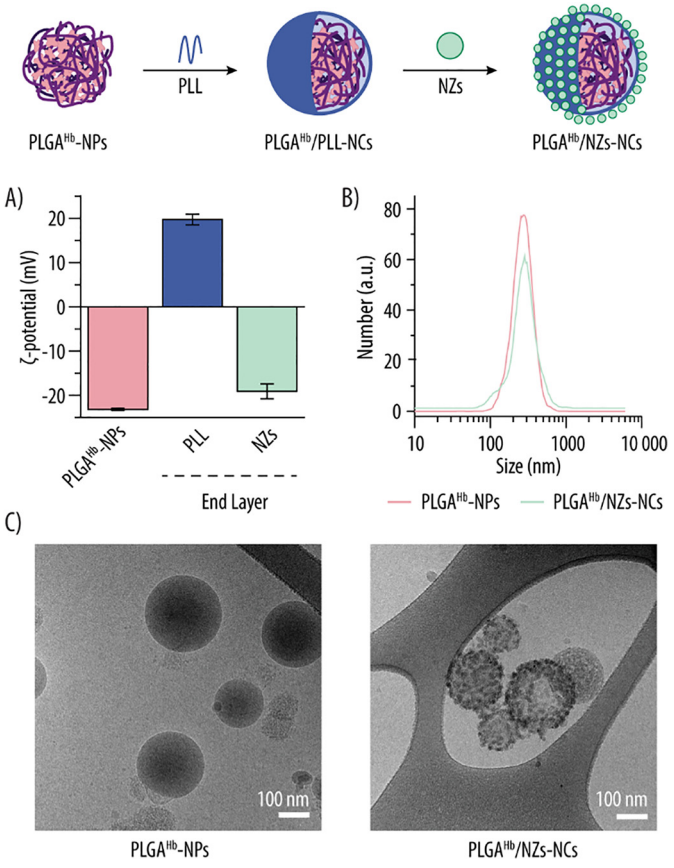

Fig. 1. Characterization of the NCs assembly. A) Zeta (ζ)-potential measurements after each step of the assembly process. B) Hydrodynamic size of bare PLGA^{Hb}-NPs and NZs-coated PLGA^{Hb}/NZs-NCs. C) CryoTEM images of PLGA^{Hb}-NPs and PLGA^{Hb}/NZs-NCs.

cancelling the NPs' stealth properties [16,34,35]. Therefore, since RBCs are nature's long circulating carriers, herein we make use of RBC-Ms as an alternative to PEG [19].

In order to obtain NCs coated with RBC-Ms, three different methods were explored (Scheme 2). For all methods, the RBC-Ms were obtained by hypotonic treatment of RBCs, which removes the intracellular contents while maintaining the integrity of the cell membranes (Scheme 2A). Herein, to obtain RBC-M, fresh blood was obtained from healthy donors, but in order to not compromise the current shortage of donor blood, in follow up work we plan to use RBC-Ms that have been extracted from outdated donor blood. As the first method, we employed the so-called extrusion method, which was pioneered by the Zhang group to coat bare PLGA-NPs and is, to date, the most commonly employed method [26,27,36]. With this protocol, the RBC-Ms are pretreated with an extrusion set to obtain RBC-MVs, which are subsequently co-extruded with the PLGA^{Hb}/NZs-NCs to render membrane-coated PLGA^{Hb}/M^{Extr}-NCs. As a second approach, the PLGA^{Hb}/NZs-NCs were coated by sonicating them together with RBC-M fragments that had been obtained by pre-sonicating the RBC-Ms. As such, it was termed the sonication method resulting in PLGA^{Hb}/M^{Sonic}-NCs. This method has also been employed to coat PLGA-NPs of several shapes or PLGA-based "nano-sponges" used to remove bacterial toxins [28,37,38]. The third and last method was recently developed in our group to coat Hb-loaded MOF-NPs to yield membrane-coated NPs with both reduced protein adsorption and in vitro cell uptake [24,29]. Specifically, the RBC-Ms are sonicated together with the PLGA^{Hb}/NZs-NCs followed by extrusion of the mixture. This approach, which uses both sonication and extrusion to yield PLGA^{Hb}/M^{Comb}-NCs, was termed as the combination method.

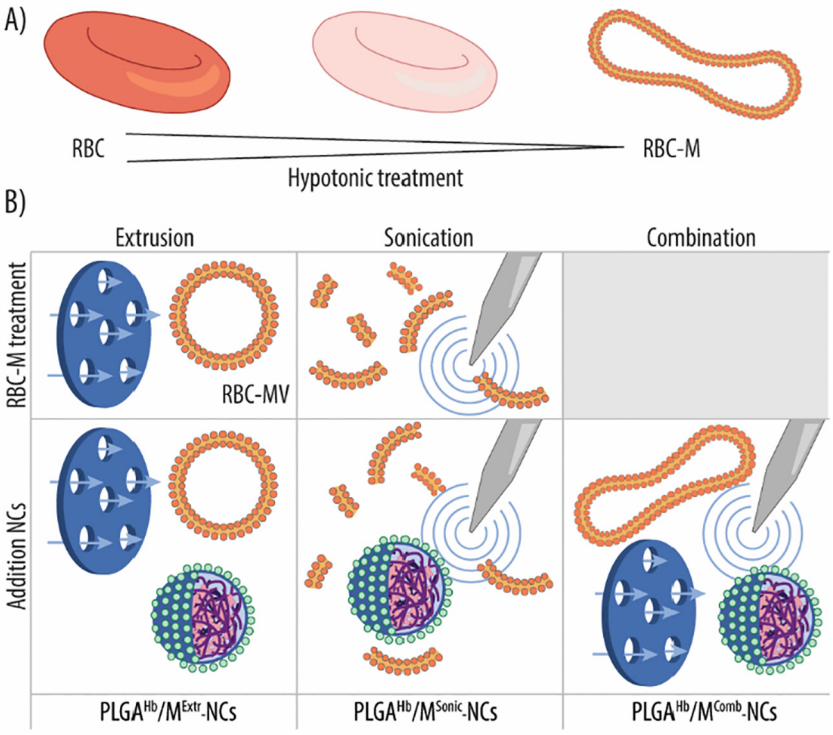

Scheme 2. Illustration of the three different membrane coating methods. A) Hypotonic treatment of red blood cells (RBCs) results in RBC-membrane (RBC-M) ghosts. B) Three methods for the coating of the NCs with RBC-Ms were employed: extrusion, sonication and the combination method. Extrusion method: extrusion is used first to obtain RBC-M vesicles (RBC-MVs) derived from the RBC-Ms and subsequently to coat the NCs with the RBC-MVs to render PLGA^{Hb}/M^{Extr}-NCs. Sonication method: sonication is used first to break the RBC-Ms into fragments and subsequently to coat the NCs with the fragments to render PLGA^{Hb}/M^{Sonic}-NCs. Combination method: to obtain PLGA^{Hb}/M^{Comb}-NCs the NCs are mixed with RBC-M, after which the suspension is sonicated and subsequently extruded to coat the NCs with the RBC-M.

Due to the negative ζ-potential of the PLGA^{Hb}/NZs-NCs, the RBC-Ms could be directly deposited onto the NCs without the need of an intermediate layer. This is due to the sialyl residues of the RBCs which render the outer surface of the RBC-M with a higher negative ζ-potential than the inner part. Due to the stronger electrostatic repulsion between the outer surface of the RBC-M and a negatively charged NC, the fusion with the RBC-Ms with the "right" side out is facilitated [27]. To determine the amount of RBC-Ms promoting the highest coverage of the NCs depending on the studied method, the PLGA^{Hb}/M-NCs were assembled with increasing amounts of fluorescently labeled RBC-M^{F}. The FI of the PLGA^{Hb}/M-NCs as a result of the fluorescent RBC-M^{F}s was evaluated by flow cytometry and, as controls, the mixture of PLGA^{Hb}/NZs-NCs and RBC-M^{F}s without any sonication or extrusion treatment, were considered (Fig. 2). For the control of the physical mixture, only a FI of ~670 could be detected upon incubation of the PLGA^{Hb}/NZs-NCs with 400 μL of RBC-M^{F} (which is the highest studied amount), while the results were very different when extrusion, sonication or the combination thereof were employed. The extrusion and the combination method gave similar results when 50–200 μL of RBC-Ms were employed. For example, when assembled using 200 μL of RBC-M^{F}s, FI readings of ~765 and ~860 were achieved for PLGA^{Hb}/M^{Extr}-NCs and PLGA^{Hb}/M^{Comb}-NCs, respectively. The highest FI readings were obtained for the sonication method reaching FI values of ~1960 and ~3180 when 200 and 400 μL of RBC-M^{F}s were used, respectively. Importantly, when using RBC-M^{F}s in the range of 100–400 μL, higher FI readings as compared to the control were obtained for the three studied methods, thus suggesting successful coverage of the NCs by the membranes.

The PLGA^{Hb}/M-NCs assembled by the three different methods were also characterized by DIC microscopy. Fig. 3 (top row) shows homogeneous and monodisperse suspensions for the three methods indicating that the NCs are individually coated, rather than multiple NCs being encapsulated within a RBC-M or a RBC-MV after the extrusion steps. This is particularly true for

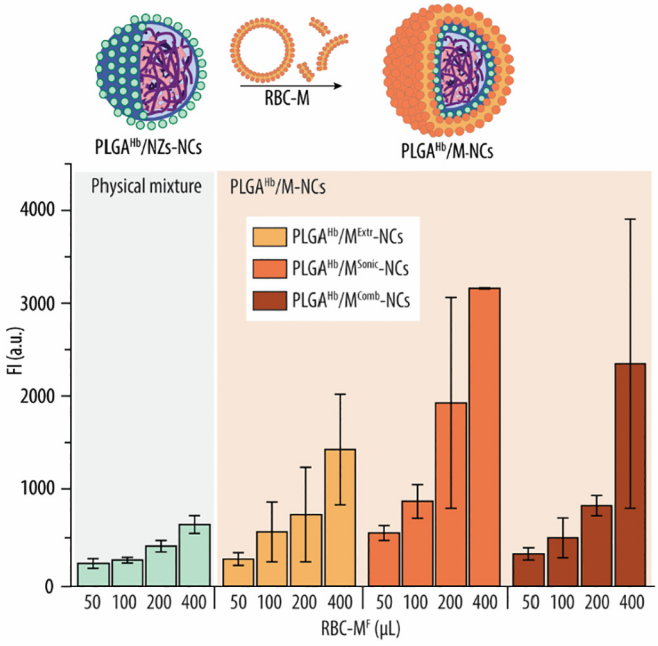

Fig. 2. Coating of the NCs with fluorescently labeled red blood cell membrane (RBC-M^{F}). Fluorescent intensity (FI) readings of NCs coated with increasing amounts of RBC-M^{F}s using the extrusion, sonication, or the combination method (PLGA^{Hb}/M^{Extr}-NCs, PLGA^{Hb}/M^{Sonic}-NCs, or PLGA^{Hb}/M^{Comb}-NCs, respectively). As controls, the physical mixtures of PLGA^{Hb}/NZs-NCs and RBC-M^{F}s (i.e., without any extrusion or sonication procedure) are considered.

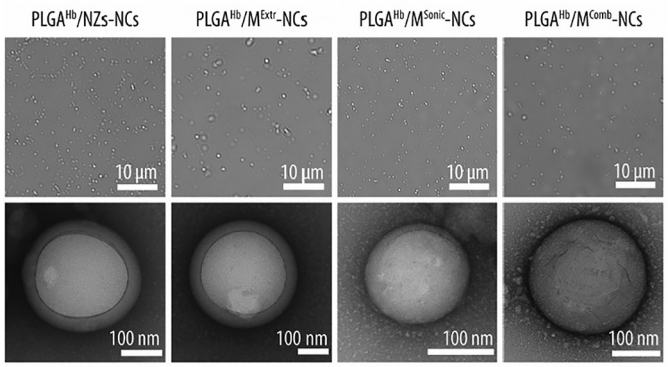

Fig. 3. Characterization of the red blood cell membrane (RBC-M)-coated NCs. Differential interference contrast images (top) and TEM images (bottom) of the NCs before (PLGA^{Hb}/NZs-NCs) or after being coated with the RBC-M employing the extrusion, sonication, or the combination method (PLGA^{Hb}/M^{Extr}-NCs, PLGA^{Hb}/M^{Sonic}-NCs, or PLGA^{Hb}/M^{Comb}-NCs, respectively).

the PLGA^{Hb}/M^{Sonic}-NCs which feature the best colloidal dispersion. The surface morphology of the PLGA^{Hb}/NZs-NCs membrane-coated PLGA^{Hb}/M-NCs depending on the coating method was assessed by TEM. For that, the NCs were stained using uranyl acetate, which acts as a negative stain by filling any void spaces, thereby enhancing the contrast of the NCs and thus revealing their structure. TEM has been previously employed by the Zhang group to characterize the coating by RBC-Ms of PLGA-NPs [27]. In their study, membrane-coated PLGA-NPs of four different sizes were imaged, all of them showing a core-shell structure that was attributed by the authors to the uniform RBC-M cloaks. Fig. 3 (bottom row) shows similar core-shell structures as the ones depicted by the Zhang group. However, since the uncoated PLGA^{Hb}/NZs-NCs control also displays a similar architecture, we can conclude that the ring present on the NCs is not an indication of successful coating by the RBC-Ms. We hypothesize that such a core-shell structure is a result of a staining artifact, where the stain is deposited between the TEM grid and the rounded bottom of the NPs, thereby darkening the outer edge of the NPs (Fig. S1, Supporting Information). Actually, if the observed dark ring by the Zhang group was a representation of the RBC-M coating, the thickness of the ring would be the same independently of the size of the PLGA-NPs. However, this is not the case since the ring observed for the smallest studied PLGA-NPs (of ~95 nm in diameter after RBC-Ms coating) is about 10 nm while, for the largest PLGA core (of ~440 nm in diameter after coating) the ring has a thickness of ~50 nm. This indicates that the artifact does not follow the added size of the RBC-M coating which, according to their DLS measurements, should be of ~10–20 nm independently of the size of the PLGA cores [27]. Interestingly, besides displaying a core-shell structure, the surfaces of the NCs also show different morphologies depending on the coating method employed. For the extrusion method, the resulting PLGA^{Hb}/M^{Extr}-NCs are very similar in morphology to their uncoated counterparts (i.e., PLGA^{Hb}/NZs-NCs). However, the NCs prepared by the combination method (i.e., PLGA^{Hb}/M^{Comb}-NCs) show a different morphology with several folds and creases, while the sonication method renders PLGA^{Hb}/M^{Sonic}-NCs with an in-between morphology of these two variants. We speculate that such morphological features could be an indication of successful coating by the RBC-Ms since the uranyl acetate anti-stain could get entrapped within the wrinkles of the membranes.

3.2. Stealth properties

The stealth properties of the RBC-M coated NCs were assessed by a protein adsorption study and solutions of albumin and immunoglobulin were used as protein models. Serum albumin is the most abundant protein in plasma and acts as a dysopsonin during early deposition, thus decreasing the recognition by the MPS [39]. However, albumin adsorption is transient and it can be easily replaced by other proteins with higher affinities, thus having an opsonic effect [39,40]. On the other hand, the γ chains of IgG are the predominant proteins adsorbed onto the NPs surface following intravenous administration, acting as potent opsonins [40]. The adsorption of these two proteins onto the PLGA^{Hb}/M-NCs assembled by the three different methods and using increasing amounts of RBC-Ms (i.e., from 100 to 800 μL) was evaluated by flow cytometry using fluorescently labeled IgG^{F} and BSA^{F} (Fig. 4). Fig. 4A shows an immediate significant decrease in IgG adsorption to ~65% nFI for the extrusion and the sonication methods (i.e., PLGA^{Hb}/M^{Extr}-NCs and PLGA^{Hb}/M^{Sonic}-NCs) as compared to the uncoated NCs (i.e., PLGA^{Hb}/NZs-NCs) for the lowest studied volume of RBC-Ms (i.e., 100 μL). The results were different for the combination method which resulted in a less efficient RBC-M coating in terms of IgG

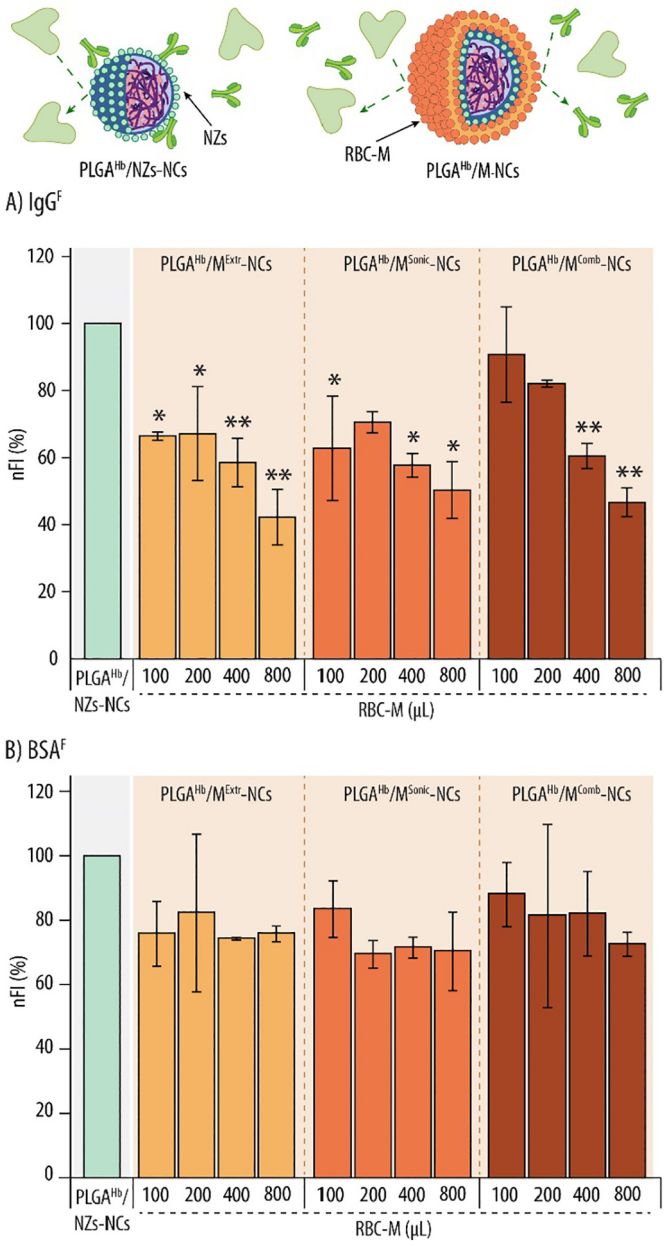

Fig. 4. Stealth properties of NCs as a result of their coating with red blood cell membrane (RBC-M). Normalized fluorescence intensity (nFI) readings due to the adsorption of fluorescently labeled immunoglobulin (IgG^{F}) (A) and serum albumin (BSA^{F}) (B) onto NCs assembled with increasing amounts of RBC-Ms employing the extrusion, sonication, or the combination method (PLGA^{Hb}/M^{Extr}-NCs, PLGA^{Hb}/M^{Sonic}-NCs, or PLGA^{Hb}/M^{Comb}-NCs, respectively). The FI readings are normalized to the uncoated PLGA^{Hb}/NZs-NCs. *$p \leq 0.05$, **$p \leq 0.01$, PLGA^{Hb}/M-NCs vs PLGA^{Hb}/NZs-NCs.

adsorption. Specifically, for PLGA^{Hb}/M^{Comb}-NCs, a significant decrease in nFI (to ~60% nFI) was only observed when 400 μL of RBC-Ms were used for the assembly. Importantly, the three studied methods rendered NCs with stealth properties since, a ~55% decrease in nFI, could be observed for the three NCs when the highest amount of RBC-Ms (i.e., 800 μL) was used for their assembly. For BSA, the results were different as shown in Fig. 4B. While for the extrusion method a ~25% decrease in nFI was already observed for the lowest RBC-Ms amount, increasing the amount of RBC-Ms (up to 800 μL) only promoted a very slight additional decrease in nFI with the lowest value being ~70% in nFI for the sonication method. We attribute this less pronounced effect of the RBC-M coating towards BSA adsorption as compared to IgG to the fact that BSA already has a weaker interaction than IgG with the uncoated PLGA^{Hb}/NZs-NCs that are used as a control. We have previously demonstrated an ~80% higher deposition of IgG onto the surface of CeO_2-NP-coated PLGA-NPs as compared to BSA; a fact that was ascribed to the electrostatic repulsion between the negative charges of BSA and CeO_2-NPs [14,41].

All in all, these results show the importance of stealth coating to minimize the adsorption of opsonins.

3.3. Oxygen binding and releasing properties

HBOCs make use of Hb's excellent O_2 carrying capacity. Therefore, the functionality of the NCs as a result of the entrapped Hb was assessed during the different steps of the NC assembly. Firstly, the secondary structure of Hb was assessed by CD analysis since protein folding is central to its function (Fig. 5). In order to encapsulate Hb within the PLGA-NPs, Hb was incorporated during their synthesis and, as such, it was exposed to an organic solvent (i.e., DCM) and sonication [15]. Additionally, the entrapment of Hb within the polymeric PLGA-NP core could influence the protein folding or coordination. Thus, the CD spectrum of PLGA^{Hb}-NPs was compared to that of free Hb (Fig. 5A). Hb has a typical α-helical secondary structure, with two negative bands around 208 and 222 nm and a positive band at 193 nm. In contrast, the spectrum of the PLGA^{Hb}-NPs shows the disappearance of the 208 nm band indicating the loss of the α-helical structures and displays a red shift and a shape that is more closely related to antiparallel β-sheets than to α-helices. Such an increase in β-sheet content can been related to protein aggregation, misfolding, or denaturation [42,43]. It should be noted that the CD data represents the average signal of the sample ensemble, which could consist of a combination of native and denatured Hb. The coating of the PLGA^{Hb}-NPs with PLL promotes a further red shift of the spectrum while the characteristic peaks of β-sheet secondary structure are maintained. PLL is a weak electrolyte that can display different conformations including random coil, α-helix or β-sheet folding depending on the pH of the solution. Fig. S2A (Supporting Information) shows that adsorption of a PLL layer onto PLGA-NPs does not lead to any change in the CD signal, but a weak, sloping signal is observed [44]. Furthermore, this is in agreement with prior results [45]. Our hypothesis is that PLL as a charged, chiral surface layer may contribute to induced CD effects or that it can penetrate into the PLGA-NPs interacting with the entrapped Hb to promote the spectral shift [46]. The deposition of the NZs causes a further shift of the spectrum towards higher wavelengths. As the NZs are achiral (Fig. S2B, Supporting Information), the change in CD is more likely due to an effect on the structure of the constituents of the PLGA^{Hb}/PLL-NCs. Fig. 5B shows the changes in the CD spectrum upon coating the NCs by RBC-Ms. The three different coating methods, namely the extrusion, sonication and the combination method were evaluated. Coating with RBC-Ms promoted a shift of the spectrum independently of the method employed. This left shift suggests an increase in α-helix content which can be attributed to the presence of proteins in the membranes extracted from the RBCs (52% of the dry weight content of RBCs corresponds to proteins). The control of RBC-Ms shows the characteristic α-helix peaks at 208 nm and 222 nm (orange dashed line). Interestingly, depending on the coating method employed, the left shifts of the spectra were more or less pronounced. The extrusion method promoted a very slight left shift while the largest shift observed was obtained for NCs coated by the sonication method. We suggest that a large change in CD spectrum could be correlated to the addition of higher amounts of RBC-M. For example, the unavoidable loss of material following an extrusion step could result in less RBC-Ms being deposited when the extrusion and the combination methods are employed. However, to support any of these hypotheses, more in-depth analysis of the different RBC-M coatings must be carried out.

Since the secondary structure of Hb seems to have been modified during the encapsulation process, we next investigated whether this change in protein folding influenced the oxygen carrying capacity of the NCs. To do so, the shifts of the Soret peak (400–440 nm region) and the Q-band (480–600 nm region) following two cycles of deoxygenation and oxygenation were evaluated. Fig. 6A shows the UV–Vis spectrum of the Hb loaded within the PLGA^{Hb}-NPs. To remove the background slope and obtain a more clear spectrum, bare PLGA-NPs were used as reference. After preparation, the PLGA^{Hb}-NPs showed the three characteristic Abs peaks of oxy-Hb. As such, a peak at ~410 nm (Soret peak) and two additional peaks at ~535 and ~575 nm (Q-band) could be observed. Following purging with N_2, a shift in both the Soret peak and the Q-band to the characteristic wavelengths of deoxy-Hb took place. Specifically, the Soret peak moved to ~428 nm while a new peak in the region of the Q-band (~560 nm) could be detected. After additional purging with compressed air and N_2, the

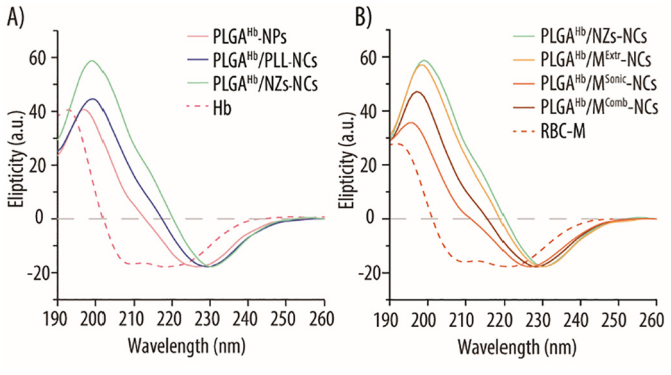

Fig. 5. Normalized CD spectra of the NCs. A) NCs at different stages of the assembly process (i.e., PLGA^{Hb}-NPs, PLGA^{Hb}/PLL-NCs and PLGA^{Hb}/NZs-NCs) using free Hb as a control. B) NCs coated by red blood cell membranes (RBC-Ms) employing the extrusion, sonication, or the combination method (PLGA^{Hb}/M^{Extr}-NCs, PLGA^{Hb}/M^{Sonic}-NCs, or PLGA^{Hb}/M^{Comb}-NCs, respectively). As controls, uncoated PLGA^{Hb}/NZs-NCs and RBC-Ms only are considered. All spectra were normalized to the lowest band of the free Hb spectrum.

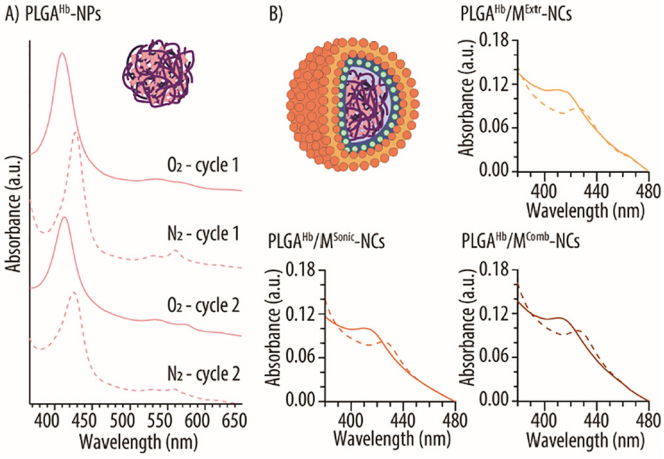

Fig. 6. Oxygen-binding and releasing properties of the NCs. A) Oxygen binding and release of PLGA^{Hb}-NPs over two consecutive cycles. B) Oxygen carrying capacity of final PLGA^{Hb}/M-NCs using the extrusion, sonication, or the combination method (PLGA^{Hb}/M^{Extr}-NCs, PLGA^{Hb}/M^{Sonic}-NCs, or PLGA^{Hb}/M^{Comb}-NCs, respectively).

corresponding shifts in the Abs peaks towards the characteristic wavelengths of oxy-Hb and deoxy-Hb, respectively, could be detected. Thus, these results indicate that despite the conformational changes, the encapsulated Hb still retained its oxygen carrying capacity. Next, to assess whether the different steps of the assembly process had any effect on the oxygen carrying ability of the final PLGA^{Hb}/M-NCs, the UV–Vis spectra of the oxygenated PLGA^{Hb}/M-NCs and after N_2 purging were monitored (Fig. 6B). While, due to the multicomponent composition of the background signal, the slopes of the spectra could not be removed, a clear shift between the oxy-Hb and deoxy-Hb states could be detected for the three PLGA^{Hb}/M-NCs, independently of the method used for the coating with the RBC-Ms.

Together, the CD and UV–Vis data confirms that eventhough the initial α-helical structure of Hb was lost, the Hb within the NCs retained its functionality.

3.4. ROS scavenging properties

Within native RBCs, Hb's ability to reversibly bind and release oxygen is protected by a multicomponent antioxidant system, which includes the SOD and CAT enzymes. This system prevents Hb from oxidation into non-functional metHb, a process that is accelerated in the presence of ROS such as $O_2^{\bullet -}$ and H_2O_2. Herein, we employ CeO_2-NPs as NZs to protect against metHb formation. CeO_2-NPs are potent NZs due to the presence of both Ce(III) and Ce(IV) oxidative states, a redox coupling that allows for the catalytic reaction with both $O_2^{\bullet -}$ and H_2O_2 [47]. While we previously showed the ability of these NZs to scavenge $O_2^{\bullet -}$ and H_2O_2, a complete comparison of these catalytic properties to those of the biological counterparts still remains to be conducted [14]. Specifically, herein, we assess the ROS scavenging properties of the NZs and the SOD and CAT enzymes following storage for up to 200 days. This is an important aspect, since HBOCs are expected to overcome the short storage shelf-life of donor blood which is only one day at RT. This presents serious logistical challenges when donor blood is required in emergencies prior to hospital admission. While SOD is known to be a stable protein, CAT loses its activity over time [48,49]. As such, herein, the aim is to compare the catalytic properties of NZs and the SOD and CAT enzymes upon long term storage at 4 °C, RT and 37 °C. As a first step, we assessed the $O_2^{\bullet -}$ and H_2O_2 scavenging properties of the NZs and the enzymes depending on the concentration. Fig. 7A shows the $O_2^{\bullet -}$ scavenging properties of both systems evaluated by means of the WST-1 assay. In this assay the $O_2^{\bullet -}$, which is produced by the xanthine/XO system, is consumed either by the WST-1 reagent or by the catalytic compound (i.e., SOD or NZs). For the former, the WST-1 is oxidized into formazan, whose Abs can be detected at 450 nm. Thus, a decrease in Abs means increased $O_2^{\bullet -}$ scavenging by the catalytic compound. Fig. 7A shows how increasing the SOD or NZs content results in decreased nAbs values, thus demonstrating the ability of the NZs to deplete $O_2^{\bullet -}$. Plateau values for $O_2^{\bullet -}$ consumption were achieved at around 0.5 mM NZs (nAbs = 4.8 ± 1.4%) and 50 U mL^{-1} SOD (nAbs = 8.1 ± 1.5%). The scavenging of H_2O_2 was investigated by the Amplex Red assay (Fig. 7B). In this assay, H_2O_2 is consumed either by Amplex Red in the presence of the HRP enzyme or by the catalytic compound (i.e., CAT or NZs). For the former, this results in the oxidation of Amplex Red into the fluorescent resorufin product ($\lambda_{ex}/\lambda_{em}$ = 530/586 nm). Thus, a decrease in FI means increased H_2O_2 scavenging by the catalytic entities. Fig. 7B shows how increased CAT or NZs content results in a decrease of the nFI values, thus demonstrating the ability of the NZs to also deplete H_2O_2. This is an important fact since this ROS is produced in the vascular tissue, but also during the reduction of $O_2^{\bullet -}$ upon auto-oxidation of Hb [5,50]. Almost complete consumption of H_2O_2 was achieved at around 0.5 mM NZs (nFI = 12.2 ± 5.5%). This nFI reading was comparable to the activity of 7.5–10 U mL^{-1} CAT (nFI = 8.5–14.7%). These results are in agreement with our previously reported catalytic activities [14]. Next, the catalytic

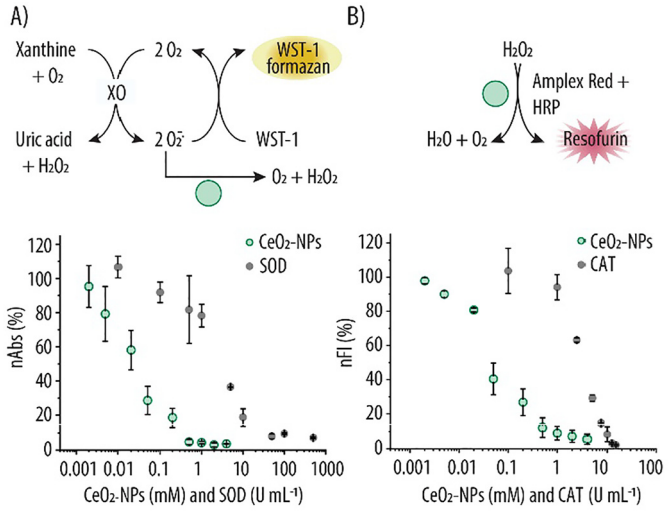

Fig. 7. Catalytic activity of NZs compared to native enzymes. A) Superoxide radical anion ($O_2^{\bullet -}$) scavenging properties of the NZs (i.e., CeO_2-NPs) and the superoxide dismutase (SOD) enzyme as measured by the WST-1 assay. The xanthine/xanthine oxidase (XO) system converts O_2 into $O_2^{\bullet -}$, where the generated $O_2^{\bullet -}$ subsequently oxidizes the WST-1 reagent into formazan (Absorbance (Abs) at 450 nm). Scavenging of $O_2^{\bullet -}$ results in a decreased amount of formazan product. B) Hydrogen peroxide (H_2O_2) scavenging properties of the NZs (i.e., CeO_2-NPs) and the catalase (CAT) enzyme as measured by the Amplex Red assay. H_2O_2 acts as a co-substrate during the conversion of Amplex Red into the fluorescent resorufin product, in presence of horseradish peroxidase (HRP). Scavenging of H_2O_2 results in a decreased amount of resorufin product (fluorescence intensity (FI) at $\lambda_{ex}/\lambda_{em}$ = 530/586 nm).

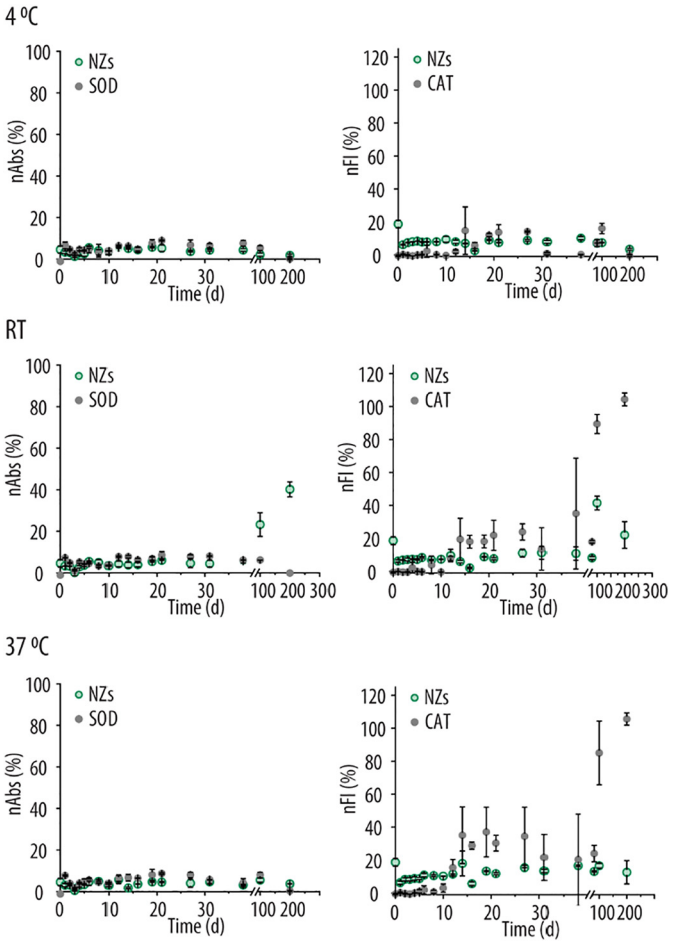

Fig. 8. Storage stability of NZs compared to native enzymes. Scavenging of the superoxide radical anion and hydrogen peroxide by the NZs or the superoxide dismutase (SOD) and catalase (CAT) enzymes upon storage up to 200 days at 4 °C, room temperature (RT) and 37 °C.

compounds were stored at 4 °C, RT and 37 °C and, at predefined time points, their catalytic activity was evaluated using the same assays (Fig. 8). As expected, due to its reported stability, SOD was able to maintain its $O_2^{\bullet -}$ scavenging properties within the whole length of the study and for the three temperature conditions. However, while the NZs were also able to maintain their catalytic activity for up to 200 days at 4 °C and 37 °C, the results were different when stored at RT. An increase in nAbs to 23% and 40% after 100 and 200 days of storage, respectively, was observed. This was thought to be due UV damage, since the NZs suspension at RT was exposed to daylight during the storage period. When looking at the scavenging properties towards H_2O_2 following long-term storage, the NZs were able to retain their activity at 4 and 37 °C. Similar to the $O_2^{\bullet -}$ scavenging, a slight loss in H_2O_2 scavenging activity was detected for NZs after 200 days when stored at RT as shown by a 22% increase in nFI. However, the results were very different for CAT where a 19% and a 35% increase in nFI was detected upon storage for only 14 days at RT and 37 °C, respectively. This decrease in scavenging activity towards H_2O_2 becomes even worse over time with a ~89% and ~85% loss in activity after 100 days of storage at RT and 37 °C, respectively. Importantly, complete loss of the CAT activity was observed at the end of the incubation period upon storage at RT and 37 °C. This highlights the potential of the NZs as a robust tool for ROS depletion.

Next, the catalytic activity of the NCs at the different stages of the assembly resulting from the adsorbed NZs was evaluated (Fig. 9). While in our previous work we reported the ROS scavenging properties of a novel HBOCs as a result of the NZs that were incorporated within the system, polydopamine, which has also ROS scavenging properties, was part of that assembly as well [29,51]. Therefore, herein, we assess the ROS scavenging properties of the NCs which arise solely from the NZs. Furthermore, the effect of the RBC-M coating on the resulting catalytic activity is evaluated. The WST-1 and Amplex Red assays were employed again to evaluate the $O_2^{\bullet -}$ (Fig. 9A) and H_2O_2 scavenging (Fig. 9B) activity, respectively. Fig. 9A shows how the PLGA^{Hb}-NPs alone promote a slight decrease in nAbs, with a maximum decrease to 82% nAbs for the highest studied amount (6×, 200 μg NPs). This is not surprising since Hb oxidizes into metHb in the presence of ROS. Following deposition of the NZs, the resulting PLGA^{Hb}/NZs-NCs promoted a marked reduction in nAbs for the four studied concentrations. For 1×, a 50% nAbs signal was detected, which was further decreased to only 6% for the highest studied concentration (i.e., 6×). This result highlights the strong antioxidant properties of this novel HBOC due to the incorporation of NZs. Following coating with the RBC-Ms to render PLGA^{Hb}/M-NCs, a slight increase in the nAbs readings for all the studied concentrations and for the three different coating methods (i.e., PLGA^{Hb}/M^{Extr}-NCs, PLGA^{Hb}/M^{Sonic}-NCs and PLGA^{Hb}/M^{Comb}-NCs) was observed. We hypothesize that this slight increase in nAbs as compared to the uncoated PLGA^{Hb}/NZs-NCs is a result of the lipid bilayer of the RBC-Ms, which hinders the diffusion of the different reactants in and out of the system. This result is not surprising since previous research in our group suggested that the RBC-M coating delays the $O_2^{\bullet -}$ scavenging properties of the underlying layer [29]. It was shown that increasing the incubation time from 30 min to 60 min removed this difference, indicating that the RBC-M coating did not affect the $O_2^{\bullet -}$ scavenging capabilities itself. The H_2O_2 scavenging by the NCs was investigated next (Fig. 9B). The PLGA^{Hb}-NPs themselves showed large consumption of H_2O_2, with an almost complete depletion for a 6× concentration (200 μg, 9% nFI). We attribute this result to the oxidation of Hb into metHb in the presence of H_2O_2 [29]. Upon incorporating the NZs, a sharp decrease in nFI is observed. This decrease in nFI is more pronounced than for the bare PLGA^{Hb}-NPs and complete H_2O_2 depletion was detected at 4× concentration (133 μg, 3% nFI). These results again highlight the strong ROS scavenging properties of the incorporated NZs. Following coating by the RBC-Ms, depending on the coating method either an increase or a decrease in nFI is detected. For example, PLGA^{Hb}/M^{Extr}-NCs promote a ~18% increase in nFI, but only for the lowest studied concentration. In contrast, PLGA^{Hb}/M^{Sonic}-NCs result on an added decrease in nFI of ~31 and ~15% for the concentrations 1× and 2×, respectively. With PLGA^{Hb}/M^{Comb}-NCs, a slight increase in nFI is again observed for the concentrations 1× and 2×. We hypothesize that these fluctuations in nFI following coating by the RBC-M could be a combination of the hindrance of the different

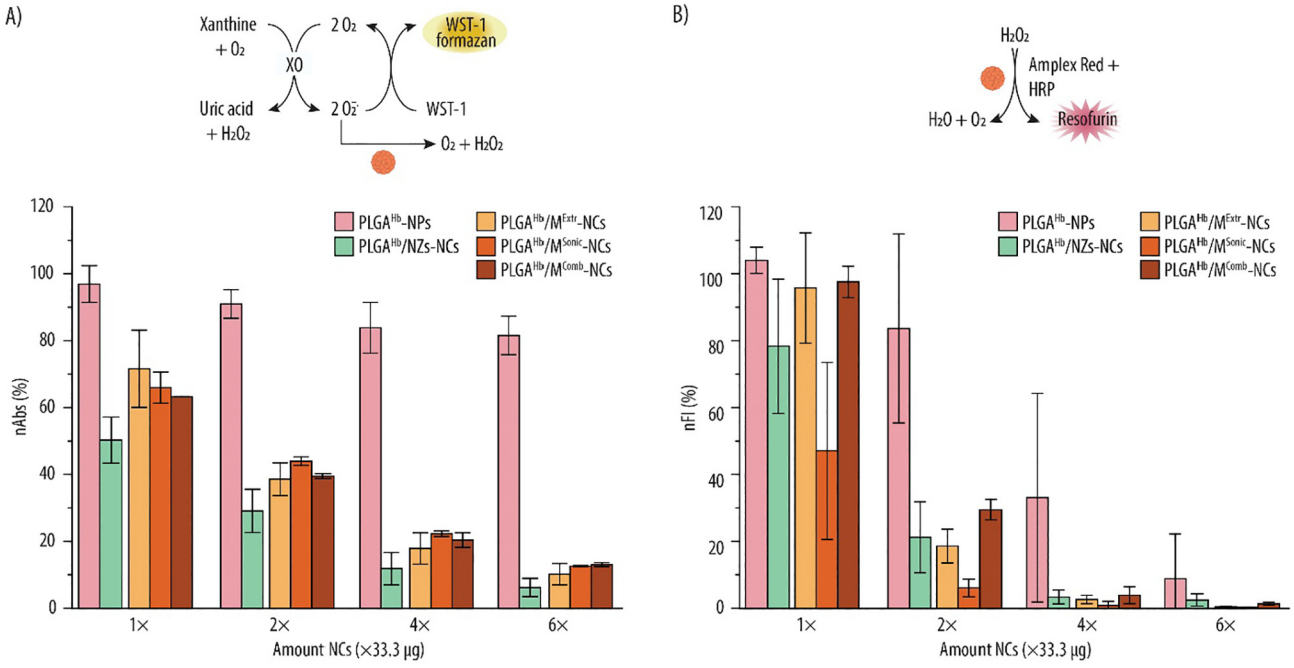

Fig. 9. Catalytic activity of the NCs. A) Superoxide radical anion ($O_2^{\bullet -}$) scavenging as measured by the WST-1 assay. The xanthine/xanthine oxidase (XO) system converts O_2 into $O_2^{\bullet -}$, where the $O_2^{\bullet -}$ subsequently oxidizes the WST-1 reagent into formazan (normalized absorbance (nAbs) at 450 nm). Scavenging of $O_2^{\bullet -}$ results in a decreased amount of formazan product. B) Hydrogen peroxide (H_2O_2) scavenging as measured by the Amplex Red assay. H_2O_2 acts as a co-substrate during the conversion of Amplex Red into the fluorescent resorufin product in the presence of horseradish peroxidase (HRP). Scavenging of H_2O_2 results in a decreased amount of resorufin product (normalized fluorescence intensity (nFI) at $\lambda_{ex}/\lambda_{em}$ = 530/586 nm). PLGA^{Hb}-NPs, PLGA^{Hb}/NZs-NCs and NCs coated with RBC-M using the extrusion, sonication, or the combination method were evaluated (PLGA^{Hb}/M^{Extr}-NCs, PLGA^{Hb}/M^{Sonic}-NCs, or PLGA^{Hb}/M^{Comb}-NCs, respectively).

reactants due to the lipid bilayer of the membranes and antioxidants from the RBCs that remained associated with the RBC-Ms. Importantly, complete depletion of the H_2O_2 was observed for the NCs independently of the coating method employed.

Next, the ability of the NCs to sustain multiple rounds of catalytic activity was investigated. For that, the catalytic reactions were conducted in a similar manner to the kinetics experiment but, after each round of catalytic activity, the samples were washed and subjected to a new reaction round. Fig. 10A shows the $O_2^{\bullet -}$ scavenging of the various NCs during four subsequent cycles. For the first cycle, using a 6× concentration (200 μg), a ~90–95% $O_2^{\bullet -}$ depletion could be detected for the PLGA^{Hb}/NZs-NCs and PLGA^{Hb}/M-NCs. After each reaction round an increase in the nAbs readings was observed, indicating partial loss of catalytic properties. This loss of activity was more pronounced for the PLGA^{Hb}/M-NCs than for the uncoated PLGA^{Hb}/NZs-NCs and was dependent on the method used to adsorb the RBC-Ms. While a ~27% in nAbs was detected for PLGA^{Hb}/M^{Extr}-NCs and PLGA^{Hb}/M^{Comb}-NCs after the fourth reaction cycle, the nAbs readings for PLGA^{Hb}/M^{Sonic}-NCs were of ~52%. While we cannot explain the differences promoted by the different coating methods, all systems still have retained more than 50% $O_2^{\bullet -}$ depletion activity even after four consecutive cycles, thereby showing the robustness of the incorporated NZs. The H_2O_2 scavenging of the NCs was also assessed over four subsequent cycles (Fig. 10B). In this case, a 4× concentration (133 μg) was evaluated since complete removal of H_2O_2 was observed at this concentration in the kinetics experiment (Fig. 9B). In the case of H_2O_2-scevenging, no marked differences were observed depending on the absence or presence of RBC-M and the coating method. Both the PLGA^{Hb}/NZs-NCs and the RBC-M-coated counterparts promoted only a ~14–24% increase in nFI after four rounds of catalytic activity. In other words, the PLGA^{Hb}/NZs-NCs and PLGA^{Hb}/M-NCs still preserved ~76–86% of the catalytic activity after the four cycles, showing the NZs' great potential in protecting Hb against H_2O_2. Furthermore, the RBC-M coating does not influence the catalytic activity of the incorporated NZs, independent of the method used.

3.5. Biocompatibility

The biocompatibility of the RBC-M-coated NCs was assessed in terms of hemolysis rate, cell viability and cell uptake/association studies to determine their potential as safe and effective nanocarrier systems.

Hemocompatibility is an important feature since the as-prepared NCs are meant to be administered intravenously and, as such, they will be in close contact with the blood cells. For that, a hemolysis rate test that measures the % of Hb release from lysed RBCs, was employed. With such a test, biomaterials are considered non-hemolytic when the hemolysis rate is less than 5% [52]. To do so, washed blood cells were exposed to the NCs prior and after RBC-M coating for 2 h. Fig. 11Ai shows how, independent of the surface coating, the NCs display hemolysis rates well below 5% for the four studies concentrations. Specifically, the hemolysis rate is ~1% for all the studied NCs, which is also the hemolysis rate of the control of blood cells only (as indicated by the dotted line). This indicates that the presence of NCs does not induce RBC lysis. The photographic images of the test tubes of the blood cells after incubation with the NCs and after being spun down are in agreement with these results (Fig. 11Aii). As such, all the tubes containing NCs show a color-less supernatant with an intact blood cell pellet and only the positive control displays a reddish supernatant that indicates the presence of free Hb.

Next, the biocompatibility of the NCs was assessed in vitro using the HUVEC endothelial cell line which was chosen as a model cell line for the endothelial cells lining in the wall of the blood vessels. For that, the cells were incubated with increasing amounts of NCs prior and after RBC-M coating and the nCV was evaluated for the three different methods (Fig. 11B). While nCV values ~100% can be observed for the lowest studied concentration (i.e., 1×), increasing amounts of NCs promoted a decrease in nCV. Specifically, a 2× concentration of NCs resulted in a ~10–20% decrease in nCV depending on the coating method. Doubling the NCs concentration to 4× promoted a further ~20 decrease in nCV for the PLGA^{Hb}/NZs -NCs and ~10% decrease for the PLGA^{Hb}/M-NCs. In contrast, further increases in the amount of NCs did not result in an additional decrease of nCV. Actually, the highest studied NCs concentration of 6× promoted a ~10% increase in nCV, however, this difference was not significantly different to the values obtained at 4× (statistics not shown). Thus, overall, good biocompatibility is observed for the lowest studied concentration of NCs and no apparent differences were observed depending on the coating method. Doubling the concentration of NCs to 2× promoted a significant decrease in nCV for the PLGA^{Hb}/NZs-NCs and PLGA^{Hb}M^{Sonic}-NCs, with increasing the amount of NCs to 4× promoting significant decreases for all four studied NCs.

To get further insight in the interaction of the coated NCs with cells, the HUVEC cell line was also employed to study the cell uptake/association of the NCs. Same concentrations of NCs were added to the cells and, following 2 h of incubation, the nCMFI was evaluated using flow cytometry. Due to the fluorescently labeled PLGA$^{F/Hb}$-NPs employed to fabricate the NCs, an increase in nCMFI can be correlated to an increase in uptake/association of the NCs with the cells. Fig. 11C shows how, as expected and in accordance with the results of Fig. 4, the bare PLGA^{Hb}/NZs-NCs resulted in highest nCMFI for all studied concentrations. For the sonication method, an average drop of ~10% in nCMFI as compared to the uncoated PLGA^{Hb}/NZs-NCs was observed for the different studied concentrations. However, interestingly, very different results were observed for the PLGA^{Hb}/

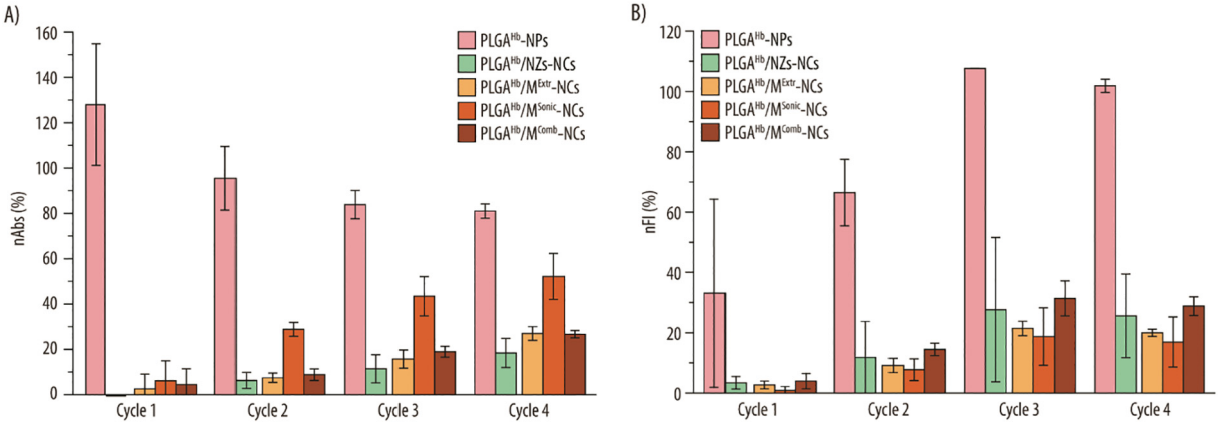

Fig. 10. NCs' catalytic activity over multiple rounds. A) Superoxide radical anion scavenging as measured by the WST-1 assay (normalized absorbance (nAbs) at 450 nm). B) Hydrogen peroxide scavenging as measured by the Amplex Red assay (normalized fluorescence intensity (nFI) at $\lambda_{ex}/\lambda_{em}$ = 530/586 nm). The assays were performed over four subsequent cycles. PLGA^{Hb}-NPs, PLGA^{Hb}/NZs-NCs and NCs coated with red blood cell membrane (RBC-M) using the extrusion, sonication, or the combination method were evaluated (PLGA^{Hb}/M^{Extr}-NCs, PLGA^{Hb}/M^{Sonic}-NCs, or PLGA^{Hb}/M^{Comb}-NCs, respectively).

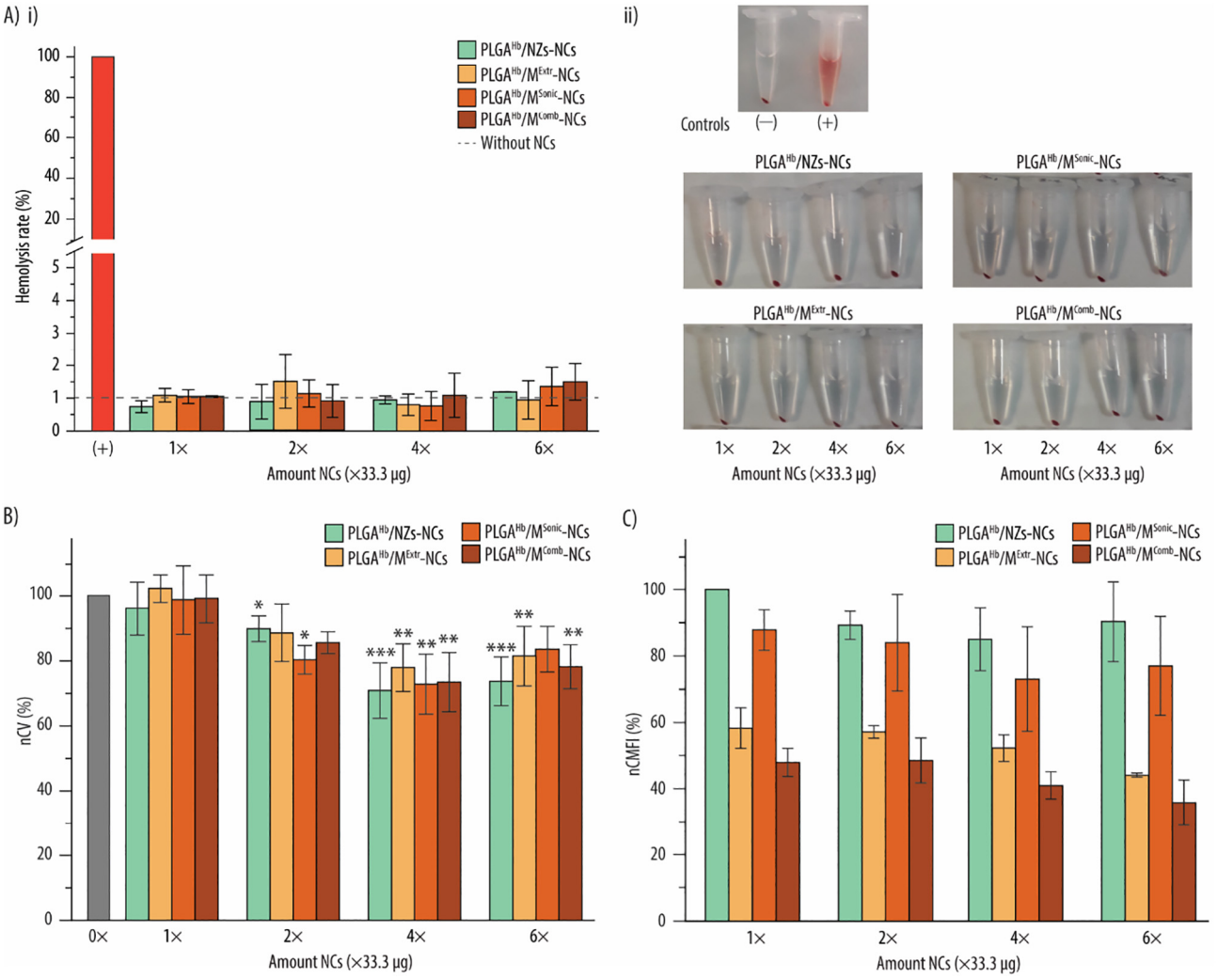

Fig. 11. The biocompatibility of the NCs. A) The hemolysis rate of NCs incubated with blood (i) and corresponding photographic images (ii). MQ and PBS were used as positive and negative controls, respectively. B) Normalized cell viability (nCV) of HUVECs incubated with increasing amounts of NCs. $*p \leq 0.05$; $**p \leq 0.01$, $***p \leq 0.001$, NCs vs 0×. C) Normalized cell mean fluorescence intensity (nCMFI) of HUVECs incubated with increasing amounts of NCs. For all studies, $PLGA^{Hb}$/NZs-NCs and NCs coated with red blood cell membrane using the extrusion, sonication, or the combination method were evaluated ($PLGA^{Hb}/M^{Extr}$-NCs, $PLGA^{Hb}/M^{Sonic}$-NCs, or $PLGA^{Hb}/M^{Comb}$-NCs, respectively).

M-NCs prepared by extrusion and combination, since these two methods promoted a very sharp and concentration-dependent decrease in nCMFI as compared to the uncoated $PLGA^{Hb}$/NZs-NCs. In particular, a ~40 and a ~50% reduction in nCMFI was observed for $PLGA^{Hb}/M^{extr}$-NCs and $PLGA^{Hb}/M^{comb}$-NCs, respectively. Such a decrease in cell association/uptake for the lowest concentration is an important aspect, since this NCs concentration showed good biocompatibility. A further increase in the NCs concentration resulted in an additional decrease in nCMFI where a ~65 and ~75% decrease in nCMFI was detected for $PLGA^{Hb}/M^{extr}$-NCs and $PLGA^{Hb}/M^{comb}$-NCs, respectively, at a NCs concentration of 6×. These results are in agreement with Fig. 4 and highlight again the importance of using membranes extracted from RBCs to provide stealth coatings. However, while the protein adsorption studies showed no obvious differences depending on the coating method employed, the results are different for cell uptake/association experiments where the sonication and combination methods render a superior stealth coating.

4. Conclusion

Successful HBOCs are required to reversibly bind and release oxygen in a sustained manner for extended periods of time. Thus, achieving long circulation in the vasculature is a crucial aspect. While surface functionalization with PEG has been the golden standard approach to achieve long circulation times, so far, its use has become under scrutiny due to the generation of anti-PEG antibodies and the subsequent clearance from the circulation. Since RBCs can remain in circulation for up to 120 days, an alternative emerging approach relies on the use of membranes extracted from RBCs. Herein, we make use of this concept to coat our previously reported HBOC consisting of Hb-loaded and NZ-decorated PLGA-NPs. For that, three different methodologies namely, the extrusion, sonication and the combination method are studied. Successful coating by the membranes is demonstrated by their ability to repel the adsorption of proteins (i.e., BSA and IgG) and to significantly decrease their uptake or association by HUVEC cells. Preservation of functionality after the coating with the RBC's membranes is demonstrated. Specifically, the coated carriers are able to carry and release oxygen and their catalytic activity resulting from the embedded NZs is demonstrated by $O_2^{\bullet -}$ and H_2O_2 depletion assays. The NZs furthermore showed long storage stability (at 4 °C, RT and 37 °C), outlasting native CAT stored at RT and 37 °C. Finally, the biocompatibility of the NCs was shown in terms of hemocompatibility and cell viability studies using HUVEC cells. Thus, to sum up, we have presented a multifaceted HBOC with potential to serve as a blood surrogate in the future.

Funding resources

This work has been supported by the Danish Council for Independent Research (Grant No. 6111-00298B) and the Lundbeck Foundation (R163-2013-15402).

Credit authorship contribution statement

Conceptualization, M.M.T.J. and L.H-R.; Experimental setup, M.M.T.J., C.C-S., X.L. and P.J.K.; Investigation and analysis, M.M.T.J., C.C-S., X.L., P.J.K. and P.W.T.; Data curation, M.M.T.J. and L.H-R.; Writing – original draft preparation M.M.T.J and L.H-R.; Writing – review and editing, M.M.T.J and L.H-R.; Visualization, M.M.T.J.; Resources, T.L.A., P.W.T. and L.H-R.; Supervision, L.H-R.; Funding acquisition, L.H-R. All authors have read and agreed to the published version of the manuscript.

Declaration of competing interest

The authors declare that they have no known competing financial interests or personal relationships that could have appeared to influence the work reported in this paper.

Appendix A. Supplementary data

Schematic of TEM anti staining and CD spectra of controls. Supplementary data to this article can be found online at https://doi.org/10.1016/j.msec.2022.112691.

References

[1] M. García-Roa, M. Del Carmen Vicente-Ayuso, A.M. Bobes, A.C. Pedraza, A. González-Fernández, M.P. Martín, I. Sáez, J. Seghatchian, L. Gutiérrez, Red blood cell storage time & transfusion: current practice, concerns & future perspectives, Blood Transfus. 15 (2017) 222–231, https://doi.org/10.2450/2017.0345-16.

[2] R.P. Rother, L. Bell, P. Hillmen, M.T. Gladwin, The clinical sequelae of intravascular hemolysis and extracellular plasma hemoglobin. A novel mechanism of human disease, JAMA 293 (2005) 1653–1662, https://doi.org/10.1001/jama.293.13.1653.

[3] J. Simoni, G. Simoni, J.F. Moeller, Intrinsic toxicity of hemoglobin: how to counteract it, Artif. Organs 33 (2009) 100–109, https://doi.org/10.1111/j.1525-1594.2008.00693.x.

[4] M.M.T. Jansman, L. Hosta-Rigau, Recent and prominent examples of nano- and microarchitectures as hemoglobin-based oxygen carriers, Adv. Colloid Interf. Sci. 260 (2018) 65–84, https://doi.org/10.1016/j.cis.2018.08.006.

[5] E. Nagababu, J.M. Rifkind, Heme degradation by reactive oxygen species, Antioxid. Redox Signal. 6 (2004) 967–978, https://doi.org/10.1089/ars.2004.6.967.

[6] F. D'Agnillo, T.M.S. Chang, Polyhemoglobin-superoxide dismutase-catalase as a blood substitute with antioxidant properties, Nat. Biotechnol. 16 (1998) 667–671, https://doi.org/10.1038/nbt0798-667.

[7] A. Alagic, A. Koprianiuk, R. Kluger, Hemoglobin-superoxide dismutase-chemical linkages that create a dual-function protein, J. Am. Chem. Soc. 127 (2005) 8036–8043, https://doi.org/10.1021/ja050339r.

[8] B. Chen, Y. Jia, J. Zhao, H. Li, W. Dong, J. Li, Assembled hemoglobin and catalase nanotubes for the treatment of oxidative stress, J. Phys. Chem. C 117 (2013) 19751–19758, https://doi.org/10.1021/jp407164q.

[9] J.M. Berg, J.L. Tymoczko, L. Stryer, Covalent modification is a means of regulating enzyme activity, in: W.H. Freeman (Ed.), Biochemistry, 5th ed., 2002 http://citeseerx.ist.psu.edu/viewdoc/summary?doi=10.1.1.201.3539. (Accessed 4 January 2019) , (New York, USA).

[10] R. Ragg, M.N. Tahir, W. Tremel, Solids go bio: inorganic nanoparticles as enzyme mimics, Eur. J. Inorg. Chem. 2016 (2016) 1906–1915, https://doi.org/10.1002/ejic.201501237.

[11] X. Liu, Y. Gao, R. Chandrawati, L. Hosta-Rigau, Therapeutic applications of multifunctional Nanozymes, Nanoscale 11 (2019) 21046–21060, https://doi.org/10.1039/c9nr06596b.

[12] M.M.T. Jansman, L. Hosta-Rigau, Cerium and iron-oxide-based nanozymes in tissue engineering and regenerative medicine, Catalysts 9 (2019) 691, https://doi.org/10.3390/catal9080691.

[13] H. Hosaka, R. Haruki, K. Yamada, C. Böttcher, T. Komatsu, Hemoglobin–Albumin cluster incorporating a Pt nanoparticle: artificial O_2 carrier with antioxidant activities, PLoS One 9 (2014), e110541, https://doi.org/10.1371/journal.pone.0110541.

[14] M.M.T. Jansman, X. Liu, P. Kempen, G. Clergeaud, T.L. Andresen, P.W. Thulstrup, L. Hosta-Rigau, Hemoglobin-based oxygen carriers incorporating nanozymes for the depletion of reactive oxygen species, ACS Appl. Mater. Interfaces 12 (2020) 50275–50286, https://doi.org/10.1021/acsami.0c14822.

[15] C. Coll-Satue, M.M.T. Jansman, P.W. Thulstrup, L. Hosta-Rigau, Optimization of hemoglobin encapsulation within Plga nanoparticles and their investigation as potential oxygen carriers, Pharmaceutics 13 (2021), https://doi.org/10.3390/pharmaceutics13111958.

[16] K. Knop, R. Hoogenboom, D. Fischer, U.S. Schubert, Poly(ethylene glycol) in drug delivery: pros and cons as well as potential alternatives, Angew. Chem. Int. Ed. 49 (2010) 6288–6308, https://doi.org/10.1002/anie.200902672.

[17] T.T.H. Thi, E.H. Pilkington, D.H. Nguyen, J.S. Lee, K.D. Park, N.P. Truong, The importance of poly(ethylene glycol) alternatives for overcoming PEG immunogenicity in drug delivery and bioconjugation, Polymers (Basel) 12 (2020) 298, https://doi.org/10.3390/polym12020298.

[18] N. d'Avanzo, C. Celia, A. Barone, M. Carafa, L. Di Marzio, H.A. Santos, M. Fresta, Immunogenicity of polyethylene glycol based nanomedicines: mechanisms, clinical implications and systematic approach, Adv. Ther. 3 (2020) 1900170, https://doi.org/10.1002/adtp.201900170.

[19] P.-A. Oldenborg, A. Zheleznyak, Y.-F. Fang, C.F. Lagenaur, H.D. Gresham, F.P. Lindberg, Role of CD47 as a marker of self on red blood cells, Science. 288 (2000) 2051–2054, https://doi.org/10.1126/SCIENCE.288.5473.2051.

[20] C.-M. Hu, R.H. Fang, L. Zhang, Erythrocyte-inspired delivery systems, Adv. Healthc. Mater. 1 (2012) 537–547, https://doi.org/10.1002/adhm.201200138.

[21] M.M. Lee-Sundlov, S.R. Stowell, K.M. Hoffmeister, M.M. Lee-Sundlov, S.R. Stowell, K.M. Hoffmeister, Multifaceted role of glycosylation in transfusion medicine, platelets, and red blood cells, J. Thromb. Haemost. 18 (2020) 1535–1547, https://doi.org/10.1111/jth.14874.

[22] L. Hosta-Rigau, B. Stadler, Shear stress and its effect on the interaction of myoblast cells with nanosized drug delivery vehicles, Mol. Pharm. 10 (2013) 2707–2712, https://doi.org/10.1021/mp4001298.

[23] W.G. Zijlstra, A. Buursma, Spectrophotometry of hemoglobin: absorption spectra of bovine oxyhemoglobin, deoxyhemoglobin, carboxyhemoglobin, and methemoglobin, Comp. Biochem. Physiol. B Biochem. Mol. Biol. 118 (1997) 743–749, https://doi.org/10.1016/S0305-0491(97)00230-7.

[24] X. Liu, M.M.T. Jansman, L. Hosta-Rigau, Haemoglobin-loaded metal organic framework-based nanoparticles camouflaged with a red blood cell membrane as potential oxygen delivery systems, Biomater. Sci. 8 (2020) 5859–5873, https://doi.org/10.1039/d0bm01118e.

[25] O.S. Ivanova, T.O. Shekunova, V.K. Ivanov, A.B. Shcherbakov, A.L. Popov, G.A. Davydova, I.I. Selezneva, G.P. Kopitsa, Y.D. Tret'yakov, One-stage synthesis of ceria colloid solutions for biomedical use, Dokl. Chem. 437 (2011) 103–106, https://doi.org/10.1134/S0012500811040070.

[26] C.-M.J. Hu, L. Zhang, S. Aryal, C. Cheung, R.H. Fang, L. Zhang, Erythrocyte membrane-camouflaged polymeric nanoparticles as a biomimetic delivery platform, Proc. Natl. Acad. Sci. U. S. A. 108 (2011) 10980–10985, https://doi.org/10.1073/pnas.1106634108.

[27] B.T. Luk, C.M. Jack Hu, R.H. Fang, D. Dehaini, C. Carpenter, W. Gao, L. Zhang, Interfacial interactions between natural RBC membranes and synthetic polymeric nanoparticles, Nanoscale 6 (2014) 2730–2737, https://doi.org/10.1039/c3nr06371b.

[28] E. Ben-Akiva, R.A. Meyer, H. Yu, J.T. Smith, D.M. Pardoll, J.J. Green, Biomimetic anisotropic polymeric nanoparticles coated with red blood cell membranes for enhanced circulation and toxin removal, Sci. Adv. 6 (2020) eaay9035, https://doi.org/10.1126/sciadv.aay9035.

[29] X. Liu, M.M.T. Jansman, W. Li, P. Kempen, P.W. Thulstrup, L. Hosta-Rigau, Metal-organic framework-based oxygen carriers with antioxidant protection as a result of a Polydopamine coating, Biomater. Sci. 9 (2021) 7257–7274, https://doi.org/10.1039/d1bm01005k.

[30] Y. Sheng, Y. Yuan, C. Liu, X. Tao, X. Shan, F. Xu, In vitro macrophage uptake and in vivo biodistribution of PLA–PEG nanoparticles loaded with hemoglobin as blood substitutes: effect of PEG content, J. Mater. Sci. Mater. Med. 20 (2009) 1881–1891, https://doi.org/10.1007/s10856-009-3746-9.

[31] X. Liu, M.M.T. Jansman, P.W. Thulstrup, A.C. Mendes, I.S. Chronakis, L. Hosta-Rigau, Low-fouling electrosprayed hemoglobin nanoparticles with antioxidant protection as promising oxygen carriers, Macromol. Biosci. 20 (2020) 1900293, https://doi.org/10.1002/mabi.201900293.

[32] R. Chandrawati, S.-F. Chong, A.N. Zelikin, L. Hosta-Rigau, B. Städler, F. Caruso, Degradation of liposomal subcompartments in Pegylated capsosomes, Soft Matter 7 (2011) 9638, https://doi.org/10.1039/c1sm05623a.

[33] D.E. Owens, N.A. Peppas, Opsonization, biodistribution, and pharmacokinetics of polymeric nanoparticles, Int. J. Pharm. 307 (2006) 93–102, https://doi.org/10.1016/j.ijpharm.2005.10.010.

[34] J.K. Armstrong, G. Hempel, S. Koling, L.S. Chan, T. Fisher, H.J. Meiselman, G. Garratty, Antibody against poly(ethylene glycol) adversely affects PEG-asparaginase therapy in acute lymphoblastic leukemia patients, Cancer 110 (2007) 103–111, https://doi.org/10.1002/cncr.22739.

[35] N.J. Ganson, T.J. Povsic, B.A. Sullenger, J.H. Alexander, S.L. Zelenkofske, J.M. Sailstad, C.P. Rusconi, M.S. Hershfield, Pre-existing anti-polyethylene glycol antibody linked to first-exposure allergic reactions to pegnivacogin, a Pegylated RNA aptamer, J. Allergy Clin. Immunol. 137 (2016) 1610–1613.e7, https://doi.org/10.1016/j.jaci.2015.10.034.

[36] C.M.J. Hu, R.H. Fang, B.T. Luk, K.N.H. Chen, C. Carpenter, W. Gao, K. Zhang, L. Zhang, "Marker-of-Self" functionalization of nanoscale particles through a top-down cellular membrane coating approach, Nanoscale 5 (2013) 2664–2668, https://doi.org/10.1039/c3nr00015j.

[37] T. Escajadillo, J. Olson, B.T. Luk, L. Zhang, V. Nizet, A red blood cell membrane-camouflaged nanoparticle counteracts streptolysin O-mediated virulence phenotypes of invasive group A streptococcus, Front. Pharmacol. 8 (2017) 477, https://doi.org/10.3389/fphar.2017.00477.

[38] Y. Chen, M. Chen, Y. Zhang, J.H. Lee, T. Escajadillo, H. Gong, R.H. Fang, W. Gao, V. Nizet, L. Zhang, Broad-spectrum neutralization of pore-forming toxins with human

erythrocyte membrane-coated nanosponges, Adv. Healthc. Mater. 7 (2018) 1701366, https://doi.org/10.1002/adhm.201701366.
[39] N. Bertrand, J.-C. Leroux, The journey of a drug-carrier in the body: an anatomo-physiological perspective, J. Control. Release 161 (2012) 152–163, https://doi.org/10.1016/j.jconrel.2011.09.098.
[40] E. AlléAaemann, P. Gravel, J.-C. Leroux, L. Balant, R. Gurny, Kinetics of blood component adsorption on poly(D,L-lactic acid) nanoparticles: evidence of complement C3 component involvement, J. Biomed. Mater. Res. 37 (1997) 229–234, https://doi.org/10.1002/(SICI)1097-4636(199711)37:2<229::AID-JBM12>3.0.CO;2-9.
[41] S. Patil, A. Sandberg, E. Heckert, W. Self, S. Seal, Protein adsorption and cellular uptake of cerium oxide nanoparticles as a function of zeta potential, Biomaterials 28 (2007) 4600–4607, https://doi.org/10.1016/j.biomaterials.2007.07.029.
[42] K. Matsuo, Y. Sakurada, R. Yonehara, M. Kataoka, K. Gekko, Secondary-structure analysis of denatured proteins by vacuum-ultraviolet circular dichroism spectroscopy, Biophys. J. 92 (2007) 4088–4096, https://doi.org/10.1529/biophysj.106.103515.
[43] P.P. Samuel, M.A. White, W.C. Ou, D.A. Case, G.N. Phillips, J.S. Olson, The interplay between molten globules and heme disassociation defines human hemoglobin disassembly, Biophys. J. 118 (2020) 1381–1400, https://doi.org/10.1016/j.bpj.2020.01.031.
[44] M. Chittchang, H.H. Alur, A.K. Mitra, T.P. Johnston, Poly(L-lysine) as a model drug macromolecule with which to investigate secondary structure and membrane transport, part I: physicochemical and stability studies, J. Pharm. Pharmacol. 54 (2002) 315–323, https://doi.org/10.1211/0022357021778556.
[45] Z. Zhi, D.T. Haynie, Direct evidence of controlled structure reorganization in a nanoorganized polypeptide multilayer thin film, Macromolecules 37 (2004) 8668–8675, https://doi.org/10.1021/ma049136y.
[46] A.M. Díez-Pascual, P.S. Shuttleworth, Layer-by-layer assembly of biopolyelectrolytes onto thermo/Ph-responsive micro/nano-gels, Materials (Basel) 7 (2014) 7472–7512, https://doi.org/10.3390/ma7117472.
[47] I. Celardo, J.Z. Pedersen, E. Traversa, L. Ghibelli, Pharmacological potential of cerium oxide nanoparticles, Nanoscale 3 (2011) 1411–1420, https://doi.org/10.1039/c0nr00875c.
[48] G.D. Mao, M.J. Poznansky, Superoxide dismutase: improving its pharmacological properties by conjugation with human serum albumin, Biomater. Artif. Cells Artif. Organs 17 (1989) 229–244, https://doi.org/10.3109/10731198909118282.
[49] M.Y. Arıca, H.A. Öktem, Z. Öktem, S.A. Tuncel, Immobilization of catalase in poly (isopropylacrylamide-co-hydroxyethylmethacrylate) thermally reversible hydrogels, Polym. Int. 48 (1999) 879–884, https://doi.org/10.1002/(SICI)1097-0126(199909)48:9<879::AID-PI237>3.0.CO;2-N.
[50] V. Kuhn, L. Diederich, T.C.S. Keller, C.M. Kramer, W. Lückstädt, C. Panknin, T. Suvorava, B.E. Isakson, M. Kelm, M.M. Cortese-Krott, Red blood cell function and dysfunction: redox regulation, nitric oxide metabolism, anemia, Antioxid. Redox Signal. 26 (2017) 718–742, https://doi.org/10.1089/ars.2016.6954.
[51] M.J. York-Duran, M. Godoy-Gallardo, M.M.T. Jansman, L. Hosta-Rigau, A dual-component carrier with both non-enzymatic and enzymatic antioxidant activity towards ROS depletion, Biomater. Sci. 7 (2019) 4813–4826, https://doi.org/10.1039/C9BM00913B.
[52] M. Lu, C. Zhao, Q. Wang, G. You, Y. Wang, H. Deng, G. Chen, S. Xia, J. Zhao, B. Wang, X. Li, L. Shao, Y. Wu, L. Zhao, H. Zhou, Preparation, characterization and in vivo investigation of blood-compatible hemoglobin-loaded nanoparticles as oxygen carriers, Colloids Surf. B 139 (2016) 171–179, https://doi.org/10.1016/j.colsurfb.2015.12.012.